



GENERAL CHARACTERISTICS AND LITHOGEOCHEMISTRY OF THE ITAGUARA LAYERED (ULTRAMAFIC-MAFIC) SEQUENCE, SOUTHERN SÃO FRANCISCO CRATON

L.E.A. Goulart, M.A. Carneiro^{1,*}

¹Departamento de Geologia; Escola de Minas, universidade Federal de Ouro Preto, Morro do Cruzeiro Campus Universitário, 35400-000, Ouro Preto, MG.

E-mail: *mauricio@degeo.ufop.br

Received para publicação em setembro de 2007, aprovado para publicação em abril de 2008

ABSTRACT

The Itaguara Layered Sequence (SAI) is a layered body of ultramafic-mafic (lherzolitic-harzburgitic, websteritic, orthopyroxenitic, gabbronoritic and gabbroic) composition, intrusive in the sialic crust of the southern portion of the São Francisco Craton (Minas Gerais, Brazil). The finer-grained varieties present mono- and polymimetic textures or, less frequently, mesocumulitic texture. The coarser-grained varieties show heteradcumulitic texture with or without intercumulus phases. The SAI lithogeochemistry characterizes it as of komatiitic affinity and corroborates to the hypothesis that the ultramafic-mafic magmatism, related to the Neoarchean Rio das Velhas Tectonothermal Event, was continuous in time and affected all the southern portion of the São Francisco Craton.

RESUMO

A Seqüência Acamada Itaguara (SAI) é um corpo acamulado de composição ultramáfica-máfica (lherzolítica-harzburgítica, websterítica, ortopiroxenítica, gabronorítica e gabróica), intrusivo na crosta siálica da porção meridional do Cráton São Francisco (Minas Gerais). As variedades mais finas apresentam textura adcumulática mono e poliminerálica ou, menos freqüentemente, textura mesocumulática. As variedades de granularidade mais grossas apresentam textura heteradcumulática com ou sem fase intercumulus. A litogeoquímica da SAI demonstra a sua afinidade komatiítica e fortalece a hipótese de que o magmatismo ultramáfico-máfico, relacionado ao Evento Tectonotermal Rio das Velhas de idade neoarqueana, foi temporalmente contínuo e espalhado por toda porção meridional do Cráton São Francisco.

INTRODUCTION

The São Francisco Craton is located in central-eastern Brazil and encompasses a crustal segment tectonically stable since the end of the Neoproterozoic, when the Brasiliano-Panafrican Orogenic Cycle terminated (Cordani *et al.*, 2000). It is informally divided in northern and southern

portions. In the latter, Archean and Proterozoic supracrustal sequences, represented by the Rio das Velhas, Minas and São Francisco supergroups, overlie an Archean sialic crust (Teixeira *et al.*, 2000). The Quadrilátero Ferrífero is inserted in this geologic context and is constituted by greenstone-type sequences and metasedimentary units of the Rio das

Velhas and Minas supergroups. The sialic crust of the southern São Francisco Craton (Figure 1) is composed of high-metamorphic grade, TTG-type (tonalite-trondhjemite-granodiorite) suites and comprises several metamorphic complexes (Carneiro, 1992, Carneiro *et al.*, 1998a, b, Endo *et al.*, 1996,

Fernandes, 2001, Machado & Carneiro, 1992, Teixeira, 1985, Teixeira *et al.*, 1996, 2000).

This crust was formed in the Mesoarchean and is related to several crustal accretion processes that occurred during its geologic evolution (Fernandes, 2001), in

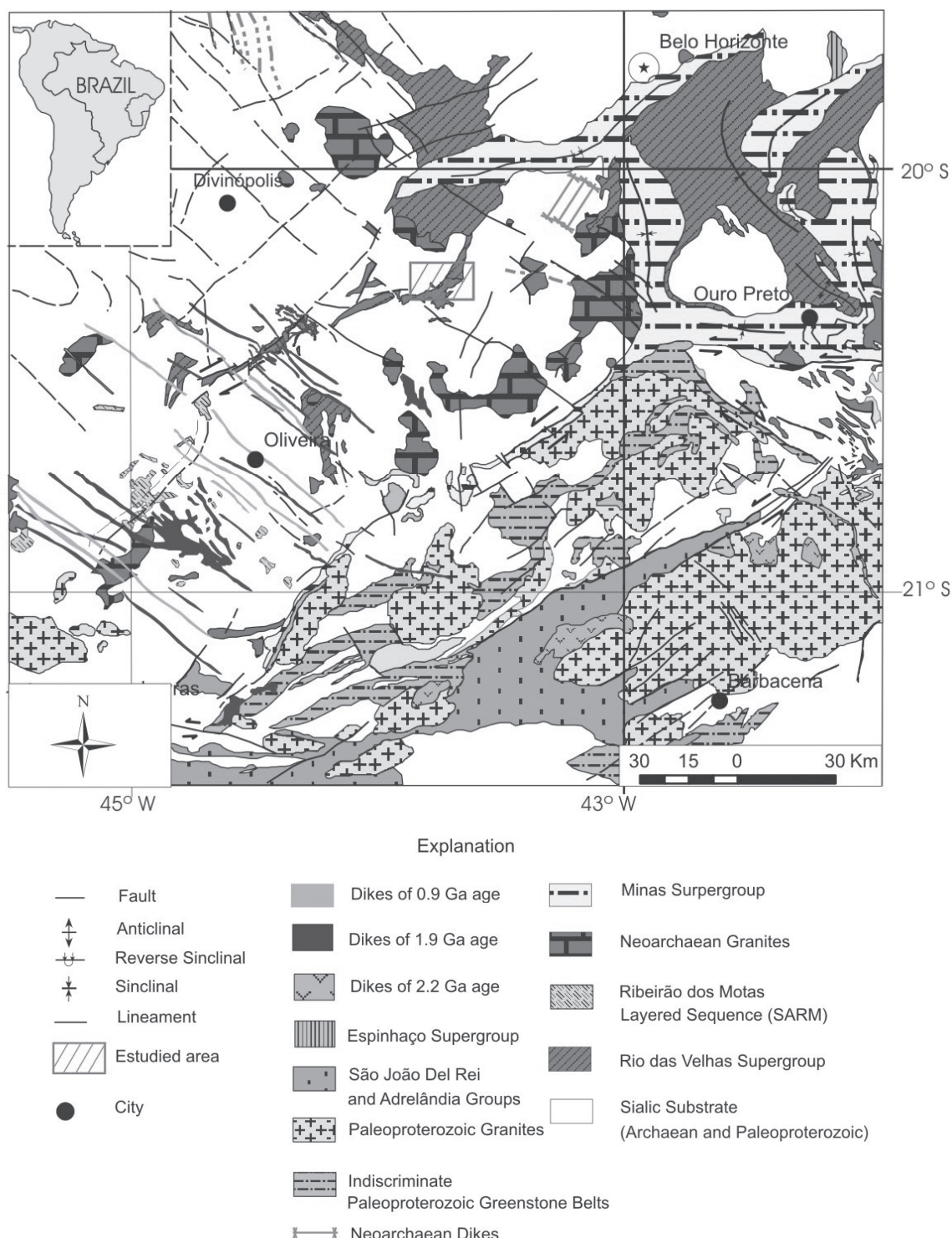


Figure 1: Geology of part of the Southern São Francisco Craton, modified after Campos (2004).

special the Rio das Velhas Tectonothermal Event (Carneiro, 1992). As products of this event, besides reworking of the sialic crust previously formed, at least two important magmatic events took place. One of them, of ultramafic-mafic nature (Padilha, 1984, Schrank *et al.*, 1990, Costa, 1995, Pinheiro, 1998, Zucchetti, 1998), generated the Rio das Velhas Supergroup basal units (SGRV - greenstone belt-type sequences), and also several bodies distributed in the southern São Francisco Craton and neighboring areas (Carneiro *et al.*, 1996, Carvalho Jr. *et al.*, 1998a,b, Carvalho Jr. & Carneiro, 1999, Carvalho Jr., 2001). Among them, the Piumhí and Fortaleza de Minas greenstone belts (Valença *et al.*, 1998, Schorscher *et al.*, 1998, Szabó, 1996) and the Ribeirão dos Motas Layered Sequence stand out (Carneiro *et al.* 1996, Carvalho Jr. *et al.* 1998a,b, Carneiro *et al.* 1999, Carvalho Jr. & Carneiro 1999, Carvalho Jr. 2001). Units similar to the Ribeirão dos Motas Layered Sequence (SARM) occur close to Cláudio and Carmópolis de Minas cities (Couto, 2004, Carneiro *et al.*, 2006, Couto & Carneiro, 2007). The other magmatic event, related to the Rio das Velhas Tectonothermal Event, is of andesitic to tholeiitic, calc-alkaline nature and is represented by granitoids and Neoarchean mafic dikes (Carneiro, 1992, Carneiro *et al.*, 1998a,b, Teixeira *et al.*, 2000, Campos *et al.*, 2003). A new occurrence of layered ultramafic-mafic magmatism has been recently identified between Itaguara and Crucilândia cities (Figure 1), apparently related to SARM (Goulart 2006). In this work a preliminary petrographic and lithogeochemical characterization of the rocks of this occurrence is presented, which is from now on named Itaguara Layered Sequence (Figure 2).

LOCATION AND GEOLOGIC SETTING

The Itaguara Layered Sequence (SAI) crops out at the Quadrilátero Ferrífero western border, in a narrow NE – SW belt (Figures 1 and 2), between Itaguara and Crucilândia. It stretches out northeastwards,

in the direction of Morro da Onça, where it is found in (undefined) contact with komatiitic flows, correlated with the Rio das Velhas Supergroup (Pinheiro, 1998). In a broad sense, SAI is intrusive in the Neoarchean sialic crust of the southern São Francisco Craton, once gneiss xenoliths are found in the rocks of this sequence. SAI also intrudes a meta-volcanosedimentary unit, whose metasedimentary portion is constituted by quartzites, sillimanite-quartzites, garnet-sillimanite-quartzites, garnet-sillimanite-schists, and, to a lesser extent, by garnet-biotite-plagioclase-quartz-schists (Goulart, 2006). The metavolcanic portion is composed of metagabbros, amphibolites and tremolite-schists. Relicts of a contact aureole are observed in the field, generated by the intrusion of SAI in metasediments. SAI is in turn (Figure 2) intruded by two (a mafic and a granitic) dike systems (Goulart, 2006). These dike systems are correlated with the mafic dikes of the Lençóis and Timboré systems (Carneiro *et al.*, 2006).

GENERAL CHARACTERISTICS AND ROCK TYPES

The Itaguara Layered Sequence (SAI) encompasses a sequence of deformed and metamorphosed ultramafic-mafic rocks (Goulart, 2006). Despite folding and faulting, its igneous layering is still preserved. This layering is characterized by a cyclic compositional variation, with thickness varying from centimeters to some meters. Not rarely, grain-size gradation occurs internally to the stratifications (Figure 3).

Under the microscope, this relict feature is composed of high metamorphic grade parageneses (amphibolite to granulite facies), which are usually in equilibrium with the cumulitic textures and primary parageneses. The primary parageneses were little affected and enable the examination of the protolith petrographic characteristics (see discussion in the next item). Another striking characteristic is the compositional variation of the SAI rock types, from peridotitic, pyroxenitic, hornblenditic and even gabbroic

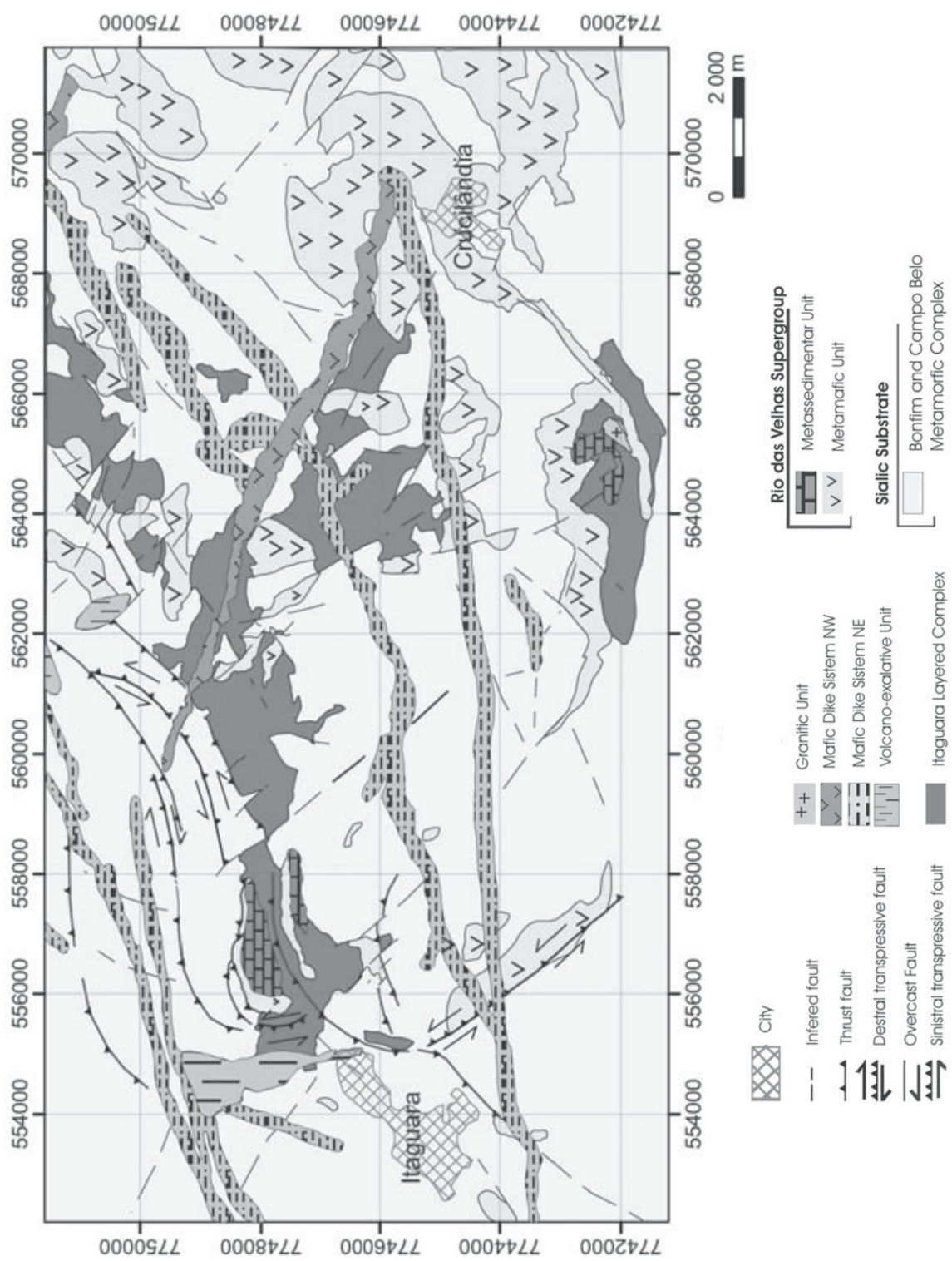


Figure 2 : Geology of the study region, modified after Goulart (2006).

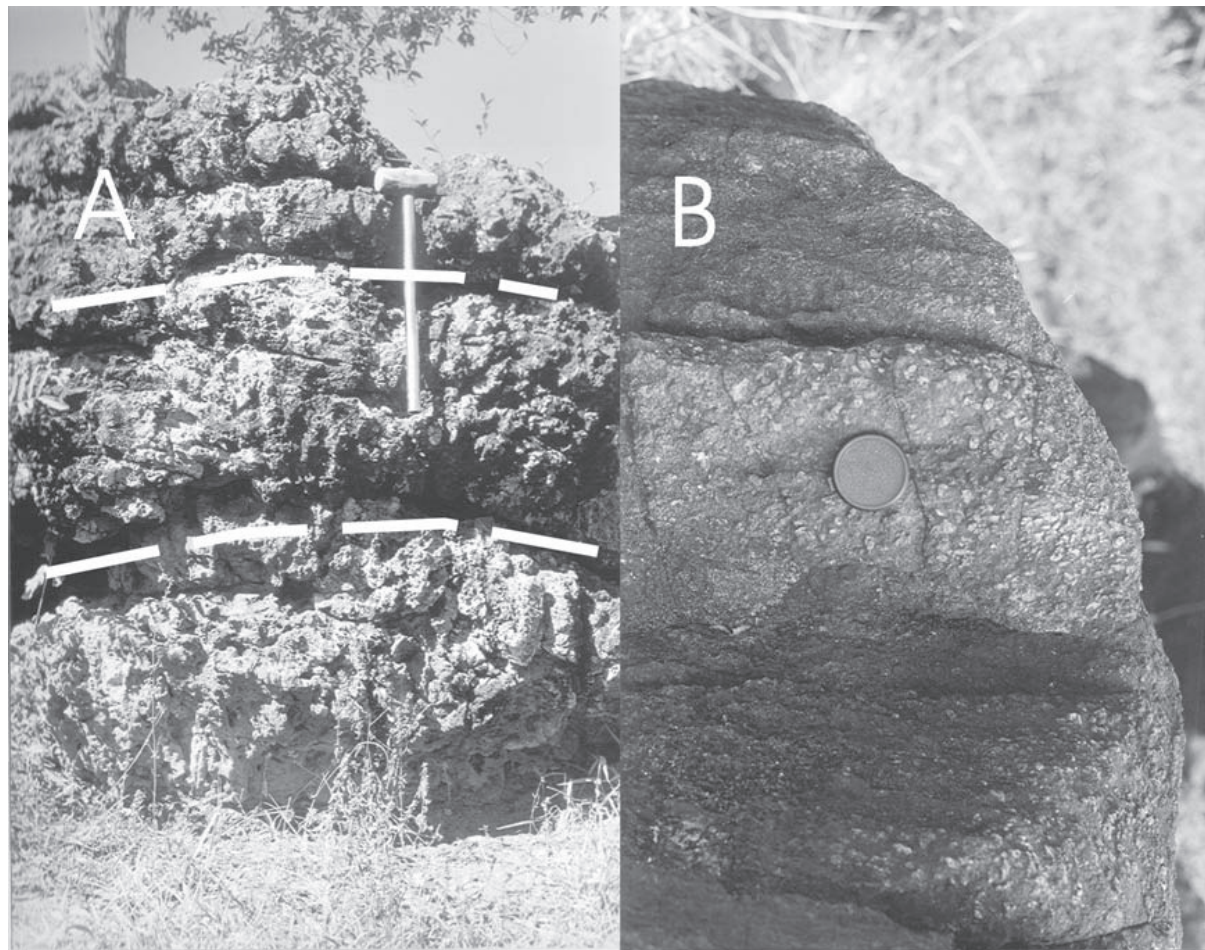


Figure 3: A) Igneous bedding of the pegmatoidal meta-orthopyroxenite: The white strips indicate bedding intervals; B) meta-harzburgite showing grain-size gradation. Photograph taken from a fold flank, where foliation crosscuts the igneous bedding at a high angle.

compositions. These varieties, as well as their petrographic characteristics are presented below.

META-PERIDOTITES

The SAI meta-peridotite varieties are meta-harzburgites and meta-lherzolites. They are characterized by alternating olivine- and pyroxene-rich, adcumulative micro-rhythms or by the presence of heteradcumulates constituted by olivine, spinels and opaque minerals, surrounded by xenomorphic orthopyroxene or, less frequently, by clinopyroxene. Locally, adcumulate relicts of olivine and orthopyroxene occur intact. These relicts are found where talcification/serpentization of olivine and orthopyroxene did not alter the textures of the primary micro-layering. These portions may or may not be associated with the nematoblastic texture

generated by the growth of amphibole at the expense of clino- and orthopyroxene. This texture is characterized by the orientation of tremolite, Mg-hornblende and, more rarely, anthophyllite, all included in ghost and/or relict orthopyroxene crystals. Although less frequent, adcumulates of olivine and spinels also occur, sometimes surrounded by clino- and orthopyroxene. Phlogopite is rare and, when present, is altered to clinochlore. The presence of tremolite and Mg-hornblende (Figure 4 A), as well as the overgrowth of green spinel (hercynite) on brown spinel, indicates that the sequence re-equilibrated at high-grade metamorphic conditions (amphibolite to granulite facies). The evidences for retrograde metamorphism are given by the overgrowth of opaque spinel (Cr-magnetite?) on the rims of zoned spinel crystals (brown nucleus/intermediate green zone/opaque rim), by the overgrowth of

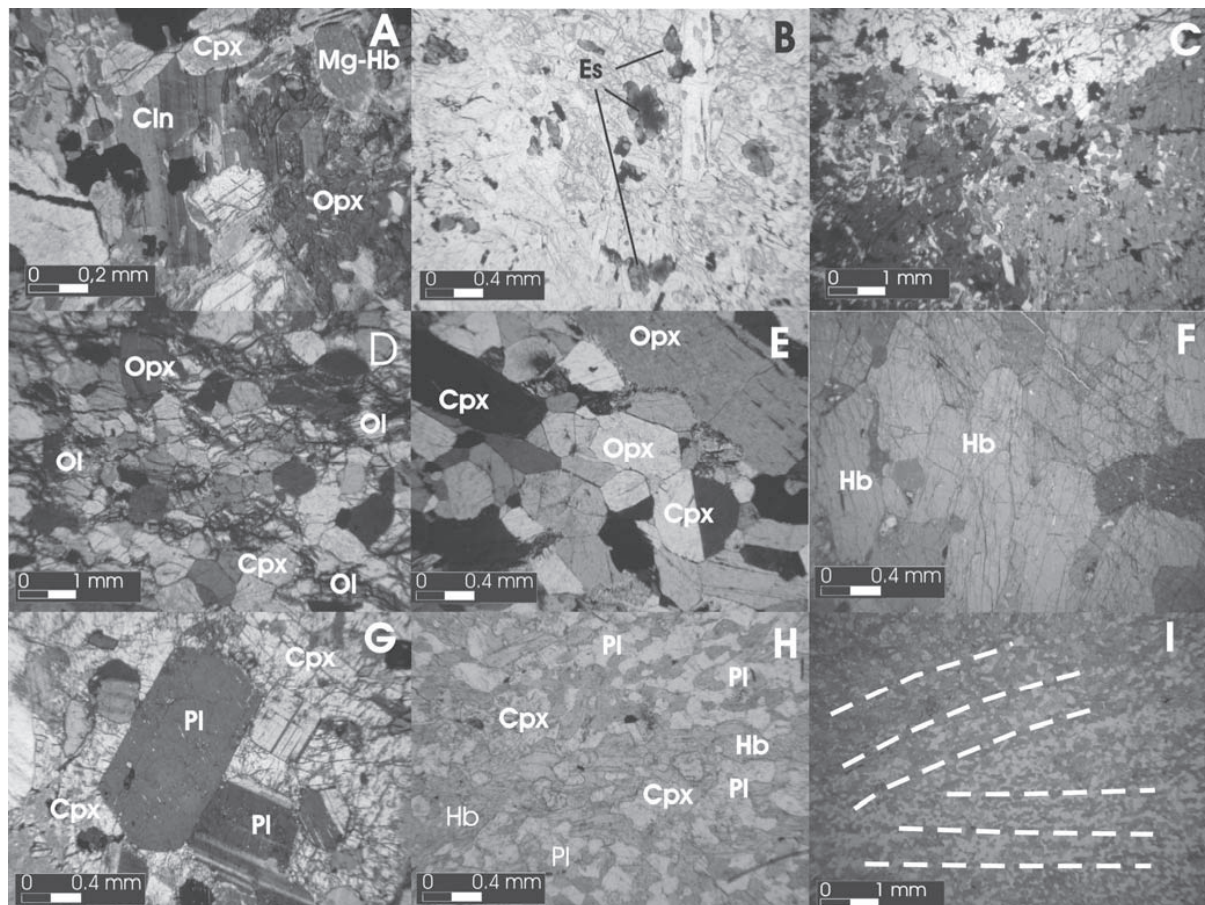


Figure 4: A) poikilo-porphyroblastic clinochlore crystal surrounding clinopyroxene, orthopyroxene, Mg-hornblende and spinel (extinct granular mineral), indicating equilibrium between mineral phases during retrograde metamorphism of meta-harzburgite (crossed polars, 10x-objective). B) Brown spinels (S.S.) showing green spinel overgrowths in meta-orthopyroxenite (plane polarized light, 10x-objective). D) Relict polymineralic adcumulitic texture defined by orthopyroxene and clinopyroxene with intercumulus olivine in meta-olivine-websterite (crossed polars, 5x-objective). C) Pegmatoidal meta-orthopyroxenite with relict heteradcumulitic orthopyroxene surrounding spinels and opaque minerals. The lepidonematoblastic matrix, formed by tremolite/Mg-hornblende, develops on a preserved igneous arrangement, the major concentrations of amphibole crystals occurring close to the contacts between orthopyroxene grains (crossed polars, 1.6x-objective). E) Equilibrium relict bimimetic adcumulitic texture defined by orthopyroxene and clinopyroxene in meta-websterite (crossed polars, 5x-objective). F) Relict adcumulitic texture defined by hornblende in hornblendite (plane polarized light, 5x-objective). G) Nucleus with heteradcumulitic texture after clinopyroxene and preserved plagioclase in metagabbro (crossed polars, 5x-objective). H) Nematoblastic texture developed on mesocumulitic texture in metagabbro (plane polarized light, 5x-objective). I) Panoramic view of previous photomicrograph. Hatched lines mark an igneous stratification formed by mesocumulate microrhythms after clinopyroxene, orthopyroxene and plagioclase, on which nematoblastic hornblende developed (plane polarized light, 1.6x-objective). Conventions: PI - plagioclase; Opx - orthopyroxene; Cpx - clinopyroxene; Ol - olivine; Hb - hornblende; Mg-Hb - Mg-hornblende; Cln - clinochlore; Es - spinel.

clinochlore on pyroxene, amphibole (Figure 4A) and phlogopite, and, in some cases, by serpentinization of olivine and talcification of orthopyroxene.

This low-grade metamorphic paragenesis (serpentine + talc + clinochlore + opaque minerals) was mainly observed in the samples obtained in fault zones and fold

hinges, suggesting that, besides a retrograde metamorphic episode, SAI was affected by some local, late-tectonic hydrothermal activity.

META-PYROXENITES

The SAI meta-pyroxenite varieties are meta-websterites, meta-olivine-websterites,

meta-olivine-orthopyroxenites and, more rarely, meta-orthopyroxenites. In respect to textures, the meta-pyroxenite grain-size varies from pegmatoid to fine. The pegmatoid varieties show relict heteradcumulitic textures with orthopyroxene including spinels and opaque minerals. This texture is usually in equilibrium with the lepidoblastic portions constituted by tremolite/Mg-hornblende that developed at the rims or fractures of large orthopyroxene crystals. In the finer-grained varieties a polymineralic adcumulitic texture predominates with orthopyroxene, clinopyroxene and olivine, this mineral also occurring in the intercumulus phase. In some varieties, adcumulitic textures with olivine grade to mesocumulates with olivine and pyroxene (Figures 4C, B, D and E), indicating gradual fractional crystallization of olivine and olivine-pyroxene. Another common feature is the sub-polygonized arrangement of ortho- and clinopyroxene crystals in equilibrium, whose contacts not rarely form angles close to 120°. In fact, the re-equilibrium under high-grade metamorphic conditions and static regime may, in some cases, have forced recrystallization at some extent; nevertheless, older igneous textures are still preserved.

META-HORNBLENDITE AND METAMAFITES

The meta-hornblendite occurs in the transition between ultramafic and mafic terms, marking the beginning of plagioclase crystallization. Plagioclase occurs as ghost crystals in the intercumulus phase of the hornblende adcumulates (Figure 4F). Despite its name, which derives from the predominant mineral (hornblende), it is possible that the original rock-forming minerals were replaced by Al-enriched varieties by means of tschermakitic substitutions during high-grade metamorphism. In this case, only the mineral morphology and the rock texture are truly igneous. Besides the tschermakitic substitution, a retrograde metamorphic paragenesis constituted by allanite + zoisite/clinozoisite + sericite, is also recognized, which corroborates to the retrograde

metamorphic processes that affected other SAI rock types. The SAI metamaflies are meta-gabbro and metagabbro. In some samples, amidst a predominantly granonematoblastic arrangement, relict nuclei are observed with heteradcumulitic texture defined by clinopyroxene (augite or hedenbergite), rimmed by plagioclase adcumulates and orthocumulates (Figure 4 G). The clinopyroxene crystals are rimmed by green hornblende, which also fills fractures internal to relict nuclei. These rocks are usually characterized by mesocumulitic textures defined by clinopyroxene, orthopyroxene and plagioclase, forming a fine igneous banding. In equilibrium with this igneous banding, a nematoblastic to granonematoblastic arrangement constituted by hornblende, plagioclase and relict pyroxene crystals (Figure 4 H and I) developed at the expense of pyroxene. Evidences of retrograde metamorphism are given by plagioclase saussuritization, development of titanite after opaque minerals (Ti-magnetite?), and, less frequently, sulfide oxidation. Completing the parageneses of these rocks, apatite occurs as accessory mineral.

METHODS

LITHOGEOCHEMISTRY

The samples used for whole-rock geochemical analyses were crushed and ground at LOPAG – Laboratory of Sample Preparation for Geochronology, Geology Department of the School of Mines, Ouro Preto Federal University. Approximately 50 g of powder from each sample were stored in sealed packs. The geochemical analyses were carried out at ACME ANALYTICAL LABORATORIES LTD. The analytical techniques used to quantify element and oxide contents and physical-chemical parameters followed the methods adopted by ACME. Powders were fused with LiBO₂ and analyzed for SiO₂, Al₂O₃, Fe₂O₃, MgO, CaO, Na₂O, K₂O, TiO₂, P2O₅, MnO, Cr₂O₃, Ni, and Sc by ICP-ES. The elements Ba, Be, Co, Cs, Ga, Hf, Nb, Rb, Sn, Sr, Ta, Th, U, V, W, Zr, Y, La, Ce,

Pr, Nd, Sm, Eu, Gd, Tb, Dy, Ho, Er, Tm, Yb, Lu were analyzed by ICP-MS. For Mo, Cu, Pb, Zn, Ni, As, Cd, Sb, Bi, Ag, Au, Hg, Tl and Se analysis by ICP-MS, the powders were digested in a solution of HCl + HNO₃ at 95° C for one hour. The results were treated and plotted in diagrams by means of the software MINPET 2.0. The program CIPW WINTER was used to calculate the CIPW norm and oxides (FeOt, FeO and Fe₂O₃), assuming that Fe₂O₃/FeO = 0.1, value suggested for basalts. Such value was adopted for the meta-ultramafites after some tests had shown that smaller values had little or no influence in the quantity of normative minerals for rock classification.

RESULTS

MOBILITY OF MAJOR ELEMENTS IN SAI

As indicated by the mineral assemblages, some chemical mobility related to major elements (e.g. Si, Ca and Mg) occurred in SAI. However, it is necessary to investigate more closely the behavior of several other elements. The results of the lithogeochemical analyses are listed in Tables 1, 2 and 3.

Figure 5 presents some diagrams using ratios between molecular proportions (RPM), as initially suggested by Pearce (1968).

For this investigation it was assumed that Fe₂O₃^t, MgO, and SiO₂ represent the main oxides involved in fractionation and differentiation of ultramafic magmas. Bivariant diagrams were generated, the chosen oxides being normalized to other oxides constituted by elements typically incompatible in magmas of this nature and of strong to relatively strong mobility under metasomatic or metamorphic conditions. Diagram 5A in Figure 5 shows a well-defined rectilinear trend. This is expected when oxides that usually behave as immobile elements, such as Fe₂O₃^t, are compared to MgO. Both are normalized to TiO₂, which is usually characterized by its low mobility. When it comes to Al₂O₃ (Figure 5B), however, the metamafites (green triangles)

and some meta-harzburgites do not follow the main rectilinear trend. While the main rock types define a more disperse trend, the contrasting group defines a secondary trend that truncates the main one. The relative Al₂O₃ mobility is also verified in the diagrams where Al₂O₃ is taken as normalizing factor. A significant dispersion occurs (Figures 5C and D), once more attesting Al₂O₃ mobility for some samples. This result evidences that this oxide may not always represent an absolute lithogeochemical pattern for the primordial magma, which may possibly be affected by post-magmatic mobilization. In these diagrams, the samples cluster in a broad strip or on two superposed lines. In Figure 5D, in particular, this mobility seems to be more intense for the more fractionated terms (metamafites, green triangles), which completely discord from the other samples. For the remaining samples, Mg may have been “concentrated” by olivine serpentinization and orthopyroxene talcification, processes that have not occurred in more Ca-enriched terms such as the metagabbro. On the other hand, Ca may have been anomalously concentrated in the metagabbro by the formation of hornblende. At a larger scale, Ca and Mg mobilization can have occurred more significantly and proportionally rather than at a sample scale, fact corroborated by the perfectly rectilinear alignment seen in Figure 5E. A similar relation is observed in the diagrams involving Si and FM (Fe₂O₃^t + MgO) - which behaves as an immobile “element” – normalized to the alkalis. The precise rectilinear trends indicate that Si and the alkalis were mobilized proportionally at body scale during high-grade metamorphism and retrograde metamorphic and metasomatic processes. Figures 5B, 5C, 5D and 5F suggest that the poorly-defined trends or the dispersion regarding TiO₂, either as normalizing factor or normalized oxide, are due to the weak Ti mobility in SAI. In these diagrams, in which the other oxides represent more easily mobilized elements, the dispersion is minimized by Ti. On the other hand, the causes for these poorly-defined alignments would also be related to

Table 1: Litogeochimistry of the SAI rock types (Mhz – meta-harzburgite; Mlz – meta-herzolite; Moopx – meta-olivine-orthopyroxenite; Mwb – meta-websterite; Mwob – meta-olivine-websterite; Mpx – meta-orthopyroxenite; Mm – metamafite). Oxide values in %.

Amostra	SiO ₂	Al ₂ O ₃	TiO ₂	Fe ₂ O ₃ ^t	MgO	CaO	Na ₂ O	K ₂ O	P ₂ O ₅	MnO	Cr ₂ O ₃	LOI	Total	Mg#	Fe ₂ O ₃	FeO ^t	FeO	
Mhz																		
AG03	42.96	8.98	0.35	11.03	23.60	5.56	0.29	0.08	0.03	0.14	0.40	6.20	99.62	72.54	1.10	9.92	8.93	
AG07	42.58	5.46	0.19	9.90	28.48	4.94	0.35	0.05	0.02	0.12	0.33	7.20	99.62	78.03	0.99	8.90	8.02	
AG08	45.71	4.58	0.20	8.92	27.64	5.08	0.12	0.05	0.01	0.12	0.39	6.70	99.52	79.28	0.89	8.02	7.22	
AG11	39.68	3.39	0.36	13.85	30.74	2.93	0.07	0.02	0.04	0.17	0.48	8.00	99.73	73.27	1.39	12.46	11.22	
AG13	40.54	3.54	0.12	9.10	34.14	1.77	0.08	0.02	0.01	0.13	0.57	9.30	99.32	82.25	0.91	8.18	7.37	
AG15	42.10	4.07	0.37	9.91	30.63	3.80	0.12	0.02	0.02	0.12	0.24	8.20	99.60	79.24	0.99	8.92	8.03	
AG16	40.57	2.94	0.30	13.35	30.63	2.92	0.04	0.02	0.02	0.20	0.20	0.36	8.20	99.55	73.91	1.34	12.01	10.81
AG22	44.04	4.90	0.20	10.44	28.49	4.73	0.28	0.03	0.06	0.14	0.44	6.00	99.75	77.12	1.04	9.39	8.45	
AG59	41.17	9.09	0.28	11.91	26.65	3.18	0.17	0.06	0.03	0.15	0.55	6.80	100.04	73.43	1.19	10.72	9.65	
AG61	41.81	5.04	0.17	9.09	31.67	2.80	0.18	0.04	0.03	0.11	0.38	8.60	99.92	81.14	0.91	8.18	7.36	
AG62	42.78	4.46	0.25	9.66	30.17	3.10	0.16	0.04	0.03	0.15	0.33	8.60	99.73	79.41	0.97	8.69	7.82	
Média	42.18	5.13	0.25	10.65	29.35	3.71	0.17	0.04	0.03	0.14	0.41	7.62	99.68	77.24	1.07	9.58	8.63	
Moopx																		
AG23	43.34	4.27	0.15	10.08	31.51	2.87	0.09	0.03	0.02	0.14	0.83	6.40	99.73	79.42	1.01	9.07	8.16	
AG25	43.49	2.96	0.11	7.22	33.68	2.81	0.09	0.02	0.03	0.13	0.31	8.80	99.65	85.21	0.72	6.50	5.85	
Média	43.42	3.62	0.13	8.65	32.60	2.84	0.09	0.03	0.03	0.14	0.57	7.60	99.72	82.32	0.87	7.79	7.01	
Mlz																		
AG01	42.05	4.36	0.16	7.28	32.65	3.53	0.08	0.02	0.01	0.11	0.31	9.10	99.66	84.70	0.73	6.55	5.90	
AG12	40.72	3.10	0.19	10.75	32.58	2.67	0.10	0.02	0.01	0.13	0.38	9.00	99.65	78.91	1.08	9.67	8.71	
AG14	43.61	4.54	0.14	8.55	33.44	1.46	0.04	0.02	0.01	0.11	0.32	7.50	99.74	82.85	0.86	7.70	6.92	
AG17	42.29	7.46	0.21	11.39	27.36	3.65	0.21	0.04	0.01	0.13	0.50	6.40	99.65	74.79	1.14	10.25	9.22	
AG19	41.18	4.06	0.14	7.60	31.62	5.05	0.09	0.02	0.01	0.14	0.33	9.50	99.74	83.71	0.76	6.84	6.15	
AG21	40.25	2.70	0.12	11.12	33.34	1.86	0.08	0.02	0.03	0.16	0.70	9.20	99.58	78.73	1.11	10.00	9.01	
AG26	38.14	4.52	0.11	8.84	34.74	1.60	0.05	0.02	0.01	0.12	0.36	11.20	99.71	82.91	0.88	7.95	7.16	
AG27	43.08	5.29	0.23	9.60	29.45	3.48	0.15	0.04	0.02	0.14	0.36	7.70	99.54	79.11	0.96	8.63	7.77	
AG36	40.15	2.95	0.11	8.02	35.92	1.06	0.01	0.02	0.02	0.11	0.29	10.09	99.56	84.69	0.80	7.22	6.49	
AG63	44.68	5.38	0.23	9.75	28.87	3.29	0.13	0.04	0.02	0.13	0.35	8.80	101.67	78.52	0.98	8.77	7.90	
Média	41.62	4.44	0.16	9.29	32.00	2.77	0.09	0.03	0.02	0.13	0.34	8.85	99.74	80.89	0.93	8.36	7.52	

Table 1: Continuation.

Amostra	SiO ₂	Al ₂ O ₃	TiO ₂	Fe ₂ O ₃ ^t	MgO	CaO	Na ₂ O	K ₂ O	P ₂ O ₅	MnO	Cr ₂ O ₃	LOI	Total	Mg#	Fe ₂ O ₃	FeO ^t	FeO	
Mwb																		
AG02	48.32	5.19	0.12	7.68	27.85	3.58	0.37	0.06	0.02	0.11	0.30	5.90	99.50	81.74	0.77	6.91	6.22	
AG04	39.64	3.98	0.13	8.43	34.55	1.94	0.05	0.02	0.01	0.11	0.29	10.50	99.65	83.50	0.84	7.58	6.83	
AG05	49.35	5.30	0.15	8.87	28.82	4.36	0.21	0.05	0.01	0.11	0.33	2.10	99.66	80.05	0.89	7.98	7.18	
AG10	39.33	5.15	0.17	9.42	32.63	3.05	0.10	0.02	0.01	0.14	0.33	9.40	99.75	81.05	0.94	8.47	7.63	
Média	44.16	4.91	0.14	8.60	30.96	3.23	0.18	0.04	0.01	0.12	0.31	6.98	99.64	81.59	0.86	7.74	6.97	
Mowb																		
AG09	48.28	5.36	0.12	7.66	27.82	3.46	0.36	0.06	0.04	0.11	0.31	6.00	99.58	81.77	0.77	6.89	6.20	
AG24	41.36	4.46	0.22	10.01	30.46	3.75	0.14	0.02	0.02	0.14	0.39	8.60	99.57	78.98	1.00	9.01	8.11	
AG58	46.91	4.32	0.25	9.38	28.09	4.96	0.32	0.06	0.03	0.13	0.36	5.20	100.01	78.71	0.94	8.44	7.59	
Média	45.52	4.71	0.20	9.02	28.79	4.06	0.27	0.05	0.03	0.13	0.35	6.60	99.73	79.82	0.90	8.11	7.30	
Mopx																		
AG18	41.28	5.62	0.18	9.12	31.71	2.81	0.08	0.02	0.03	0.12	0.33	8.40	99.70	81.11	0.91	8.21	7.39	
AG20	42.51	3.70	0.15	7.98	33.06	2.42	0.03	0.02	0.02	0.12	0.34	9.50	99.85	83.65	0.80	7.18	6.50	
AG32	46.65	6.21	0.19	10.34	28.08	3.40	0.16	0.02	0.06	0.18	0.41	4.10	99.80	77.03	1.03	9.30	8.37	
Média	43.48	5.18	0.17	9.15	30.95	2.88	0.09	0.02	0.04	0.14	0.36	7.33	99.79	80.60	0.91	8.23	7.42	
Mm																		
AG28	48.56	14.07	1.14	13.53	7.10	10.32	3.19	0.82	0.12	0.20	0.02	0.70	99.77	38.82	1.38	12.17	11.19	
AG29	51.00	13.38	1.59	14.63	5.81	9.56	2.47	0.42	0.15	0.23	0.01	0.50	99.75	32.46	1.49	13.16	12.09	
Média	49.78	13.73	1.37	14.08	6.46	9.94	2.83	0.62	0.14	0.22	0.01	0.60	99.78	35.64	1.44	12.67	11.64	

Table 2: Litogeochemistry of the SAI rock types (Mhz – meta-harzburgite; Mlz – meta-lherzolite; Moopx – meta-olivine-orthopyroxenite; Mwb – meta-websterite; Mwob – meta-olivine-websterite; Mpx – meta-orthopyroxenite; Mm – metabasite). Concentrations in ppm, except for Au, which is given in ppb.

Amostra	Mo	Cu	Cr	Pb	Zn	As	Cd	Sb	Bi	Ag	Au	Hg	Tl	Se	Ba	Ni	Sc	Co	Cs	Ga	Hf	Nb
Mhz																						
AG03	0.10	4.00	2757.33	1.70	17.00	1.60	0.10	0.10	0.10	0.50	0.01	0.10	0.50	17.00	1036.00	29.00	101.40	1.70	7.90	1.00	1.20	
AG07	0.10	2.30	2223.65	0.50	11.00	2.50	0.10	0.10	0.10	0.50	0.01	0.10	0.50	25.00	1131.00	16.00	109.80	1.30	4.40	0.50	1.30	
AG08	0.10	6.10	2661.54	5.60	11.00	0.50	0.30	0.10	0.20	0.10	0.50	0.01	0.10	0.50	38.00	2870.00	18.00	107.60	2.30	4.70	0.50	0.60
AG11	0.10	0.70	3277.32	0.40	24.00	0.50	0.10	0.10	0.10	0.50	0.01	0.10	0.50	23.00	1765.00	12.00	156.10	0.40	5.30	0.80	2.40	
AG13	0.10	2.20	3893.10	1.50	13.00	8.10	0.10	0.10	0.30	0.10	0.60	0.01	0.10	0.50	7.00	1994.00	14.00	121.80	2.60	3.80	0.50	0.50
AG15	0.10	1.90	1635.24	0.50	16.00	2.20	0.10	0.10	0.20	0.10	26.80	0.01	0.10	0.50	26.00	1796.00	15.00	112.10	0.70	5.00	0.80	1.40
AG16	0.10	158.80	2456.28	4.00	27.00	0.80	0.10	0.10	0.20	0.20	0.50	0.01	0.10	0.50	6.00	1990.00	12.00	155.70	0.90	4.50	0.60	1.60
AG22	0.10	8.00	2989.95	0.20	10.00	0.50	0.10	0.10	0.10	0.50	0.01	0.10	0.50	15.00	1325.00	21.00	110.00	0.60	6.40	0.50	0.50	
AG59	0.10	2.40	3728.89	0.50	11.00	1.50	0.10	0.10	0.10	0.50	0.01	0.10	0.50	5.70	903.00	29.00	98.20	2.30	8.20	0.50	0.50	
AG61	0.10	2.00	2613.64	0.40	16.00	25.20	0.10	0.10	0.30	0.10	0.50	0.01	0.10	0.50	0.70	1998.00	16.00	96.00	2.80	4.30	0.50	0.70
AG62	0.40	2.40	2278.39	0.80	20.00	4.90	0.10	0.10	0.10	0.50	0.01	0.10	0.50	5.10	1797.00	16.00	92.80	2.20	4.40	0.50	0.80	
Média	0.13	17.35	2774.12	1.46	16.00	4.39	0.12	0.10	0.16	0.11	2.90	0.01	0.10	0.50	15.32	1691.36	18.00	114.68	1.62	5.35	0.61	1.05
Moopx																						
AG23	0.10	1.70	5678.86	0.60	17.00	7.90	0.10	0.10	0.10	1.90	0.01	0.10	0.50	13.00	1410.00	16.00	119.30	2.60	5.20	0.50	0.50	
AG25	0.10	7.50	2134.70	0.70	7.00	8.50	0.10	0.10	0.30	0.10	0.50	0.01	0.10	0.50	8.00	2289.00	13.00	103.80	0.60	3.10	0.50	0.50
Média	0.10	4.60	3906.78	0.65	12.00	8.20	0.10	0.10	0.20	0.10	1.20	0.01	0.10	0.50	10.50	1849.50	14.50	111.55	1.60	4.15	0.50	0.50
Mlz																						
AG01	0.10	4.40	2121.02	0.60	16.00	0.50	0.10	0.10	0.40	0.10	0.50	0.01	0.10	0.50	17.00	1522.00	14.00	104.80	1.70	3.90	0.50	1.20
AG12	0.10	22.40	2599.96	1.30	17.00	0.50	0.10	0.10	0.10	0.70	0.01	0.10	0.50	9.00	1873.00	13.00	121.20	1.10	2.90	0.50	0.50	
AG14	0.10	9.90	2203.12	0.90	12.00	30.50	0.10	0.10	0.10	0.10	3.30	0.01	0.10	0.50	37.00	1864.00	16.00	109.70	3.80	4.20	0.50	0.70
AG17	0.10	11.70	34.21	0.50	4.00	0.50	0.10	0.10	0.10	0.50	0.01	0.10	0.50	21.00	1233.00	25.00	118.40	3.10	8.10	0.50	0.50	
AG19	0.10	9.40	2285.23	0.20	15.00	1.00	0.10	0.10	0.10	0.50	0.01	0.10	0.50	11.00	1340.00	15.00	97.70	0.90	3.60	0.50	0.50	
AG21	0.10	0.20	4768.87	2.10	8.00	2.10	0.10	0.10	0.10	0.50	0.01	0.10	0.50	15.00	1306.00	15.00	122.60	5.00	3.20	0.50	0.50	
AG26	0.10	0.70	2442.59	0.20	14.00	18.50	0.10	0.10	0.10	2.80	0.01	0.10	0.50	9.00	1802.00	13.00	102.90	0.70	4.60	0.50	0.60	
AG27	0.10	4.00	2456.28	0.70	14.00	43.50	0.10	0.10	0.40	0.10	9.20	0.01	0.10	0.50	62.00	1576.00	20.00	105.40	1.30	6.20	0.50	0.70
AG36	0.10	0.70	1970.50	0.10	16.00	0.70	0.10	0.10	0.10	0.50	0.01	0.10	0.50	9.00	2029.00	12.00	114.10	0.40	3.30	0.50	0.50	
AG63	0.10	0.90	2381.02	0.40	11.00	0.80	0.10	0.10	0.10	0.50	0.01	0.10	0.50	0.90	1615.00	16.00	87.80	3.40	5.50	0.50	0.80	
Média	0.10	6.43	2326.28	0.70	12.70	9.86	0.10	0.10	0.16	0.10	1.90	0.01	0.10	0.50	19.09	1616.00	15.90	108.46	2.14	4.55	0.50	0.65

Table 2: Continuation

Amostra	Mo	Cu	Cr	Pb	Zn	As	Cd	Sb	Bi	Ag	Au	Hg	Tl	Se	Ba	Ni	Sc	Co	Cs	Ga	Hf	Nb
Mwb																						
AG02	0.30	39.80	2045.76	0.80	20.00	0.50	0.10	0.60	0.10	0.50	0.01	0.20	0.50	10.00	1112.00	17.00	93.40	0.80	6.10	0.50	0.60	
AG04	0.10	0.40	1956.81	0.20	12.00	4.70	0.10	0.10	0.10	0.50	0.01	0.10	0.50	14.00	1624.00	12.00	117.10	0.50	4.10	0.50	0.70	
AG05	0.10	0.30	2257.86	0.50	2.00	3.30	0.10	0.10	0.10	0.70	0.01	0.10	0.50	5.00	1295.00	14.00	109.00	1.40	7.60	0.50	0.90	
AG10	0.10	4.50	2257.86	1.10	22.00	26.30	0.10	0.10	0.10	0.70	0.01	0.10	0.50	9.00	1635.00	16.00	115.10	1.60	5.30	0.50	1.00	
Média	0.15	11.25	2129.57	0.65	14.00	8.70	0.10	0.10	0.23	0.10	0.60	0.01	0.13	0.50	9.50	1416.50	14.75	108.65	1.08	5.78	0.50	0.80
Mowb																						
AG09	0.20	35.30	2148.39	2.00	23.00	0.60	0.10	0.10	0.50	0.10	0.50	0.01	0.10	0.50	21.00	1119.00	17.00	97.30	0.90	6.40	0.50	0.80
AG24	0.10	1.80	2634.17	0.70	18.00	139.50	0.10	0.20	0.40	0.10	32.00	0.01	0.10	0.50	125.00	2298.00	17.00	117.80	0.70	5.30	0.50	0.70
AG58	0.20	11.20	2490.49	0.30	15.00	3.30	0.10	0.10	0.20	0.10	0.50	0.01	0.10	0.50	19.60	1728.00	15.00	94.70	2.10	4.80	0.70	1.40
Média	0.17	16.10	2424.35	1.00	18.67	47.80	0.10	0.13	0.37	0.10	11.00	0.01	0.10	0.50	55.20	1738.33	16.33	103.27	1.23	5.50	0.57	0.97
Mopx																						
AG18	0.10	8.40	2244.18	0.60	14.00	0.50	0.10	0.10	0.10	0.50	0.01	0.10	0.50	11.00	1680.00	18.00	108.50	3.10	5.80	0.50	0.70	
AG20	0.10	2.50	2333.12	0.50	9.00	0.50	0.10	0.10	0.10	0.50	0.01	0.10	0.50	16.00	1774.00	16.00	105.30	0.70	3.50	0.50	0.50	
AG32	0.10	58.30	2777.85	0.10	5.00	0.70	0.10	0.10	0.10	0.70	0.01	0.10	0.50	5.00	1348.00	22.00	109.10	1.20	7.30	0.50	0.50	
Média	0.10	23.07	2451.72	0.40	9.33	0.57	0.10	0.10	0.10	0.57	0.01	0.10	0.50	10.67	1600.67	18.67	107.63	1.67	5.53	0.50	0.57	
Mm																						
AG28	0.10	25.90	157.37	0.50	19.00	0.50	0.10	0.10	0.10	0.60	0.01	0.10	0.50	58.00	100.00	45.00	65.80	0.40	16.60	1.80	3.70	
AG29	0.20	79.20	47.89	0.70	20.00	0.50	0.10	0.10	0.10	0.60	0.05	0.10	0.50	102.00	55.00	48.00	79.60	0.70	20.00	2.40	7.10	
Média	0.15	52.55	102.63	0.60	19.50	0.50	0.10	0.10	0.10	0.60	0.03	0.10	0.50	80.00	77.50	46.50	72.70	0.55	18.30	2.10	5.40	

the relative Ti concentration in space and time, as a result of re-distribution of the more mobile elements at a body scale. The mobility pattern for SAI, in a decreasing order, would be: Na>K>Si>Al>Mg>Ti. Regarding the Mg mobility, it may have been less important at a sample scale, having in mind the presence of relict cumulitic textures, where the primary parageneses are preserved. At a body scale, it is probable that Mg mobility was chaotic, rather than linear, mainly when it was related to deformation at fold axes and/or shear zones. In this case, Mg concentrations may have been a consequence of the interaction of the rock with metasomatic liquids (serpentization and talcification). Therefore for the majority of the samples and in respect to the $\text{TiO}_2/\text{Al}_2\text{O}_3$ ratios, SAI presents reasonably reliable records of the geochemical patterns of the parental magma. Doubts still remain regarding the $\text{CaO}/\text{Al}_2\text{O}_3$ ratios, due to the extreme Ca mobility, as well as the geochemical patterns regarding de K and Na concentrations.

BEHAVIOR OF OXIDES AND MAJOR AND TRACE ELEMENTS IN SAI.

As already discussed, Mg is relatively mobile in SAI rocks. Possibly this mobility is more proportional when observed at a body rather than a sample scale. Moreover, the relict cumulitic textures formed by olivine and orthopyroxene point to the significant role played by Mg during fractionation of the parental ultramafic magmas. Therefore MgO is adopted as the variation index in the bivariate diagrams of Figures 6 and 7.

The diagrams show that the incompatibility of SiO_2 , TiO_2 , Al_2O_3 , total alkalis ($\text{Na}_2\text{O} + \text{K}_2\text{O}$), Fe_2O_3 is conspicuous and concurs with the Mg-olivine, orthopyroxene, spinel and sulfide fractionation during the magnesian magma differentiation. A similar behavior is observed for highly incompatible elements, such as V, Cu, Rb, Sc, Zr and Y, which in Figure 6, define negative trends in relation to MgO. The immobility of e.g. Sc, V, Zr and Y, in opposition to the negative

trends in relation to MgO, would be a first, important record of the differentiation/fractionation episodes of the SAI primordial, parental magmas. However, the Y x MgO diagram shows an anomalous enrichment for some samples, which possibly resulted from assimilation of crustal components, either by contamination of the mantle source with subducted material or during magma ascension to the crust. Compatible elements, in particular Co and Ni, define positive trends versus MgO. This behavior suggests certain immobility in face of metamorphic/metasomatic processes that altered the original chemical composition of the rocks. It is also suggestive of the existence of primary sulfide deposits in SAI. A striking behavior is observed for Cr. For MgO contents larger than ca. 25%, Cr behaves as an incompatible element, whereas for $\text{MgO} < 25\%$, it behaves as a compatible element. This implies that during magma fractionation, for instance, the crystallization of chromite would only start when MgO contents would decrease to 25% in the residual magma. Irvine (1975, 1977) shows that chromite can crystallize together with olivine when fractionation of a primitive magma begins. Chromite would, together with orthopyroxene and olivine, be a fundamental phase in the differentiation of the SAI magnesian magmas. A similar Cr versus MgO relation was observed in many other classic komatiite occurrences such as Barbeton (Smith *et al.* 1980) and Ylgarn (Binns *et al.* 1982). These facts support a possible komatiitic filiation for the SAI parental magmas.

GENERAL CHARACTERISTICS OF THE GEOCHEMICAL PATTERNS AND THE ANOMALOUS REE ENRICHMENT.

Figure 8A shows that some of the SAI rocks are more fractionated in respect to chondritic values. Strong negative Pb anomalies associated with minor negative Nb, Ce, Sr and Zr anomalies and positive Cs, Ba, U, Nd and Y anomalies characterize the SAI geochemical pattern.

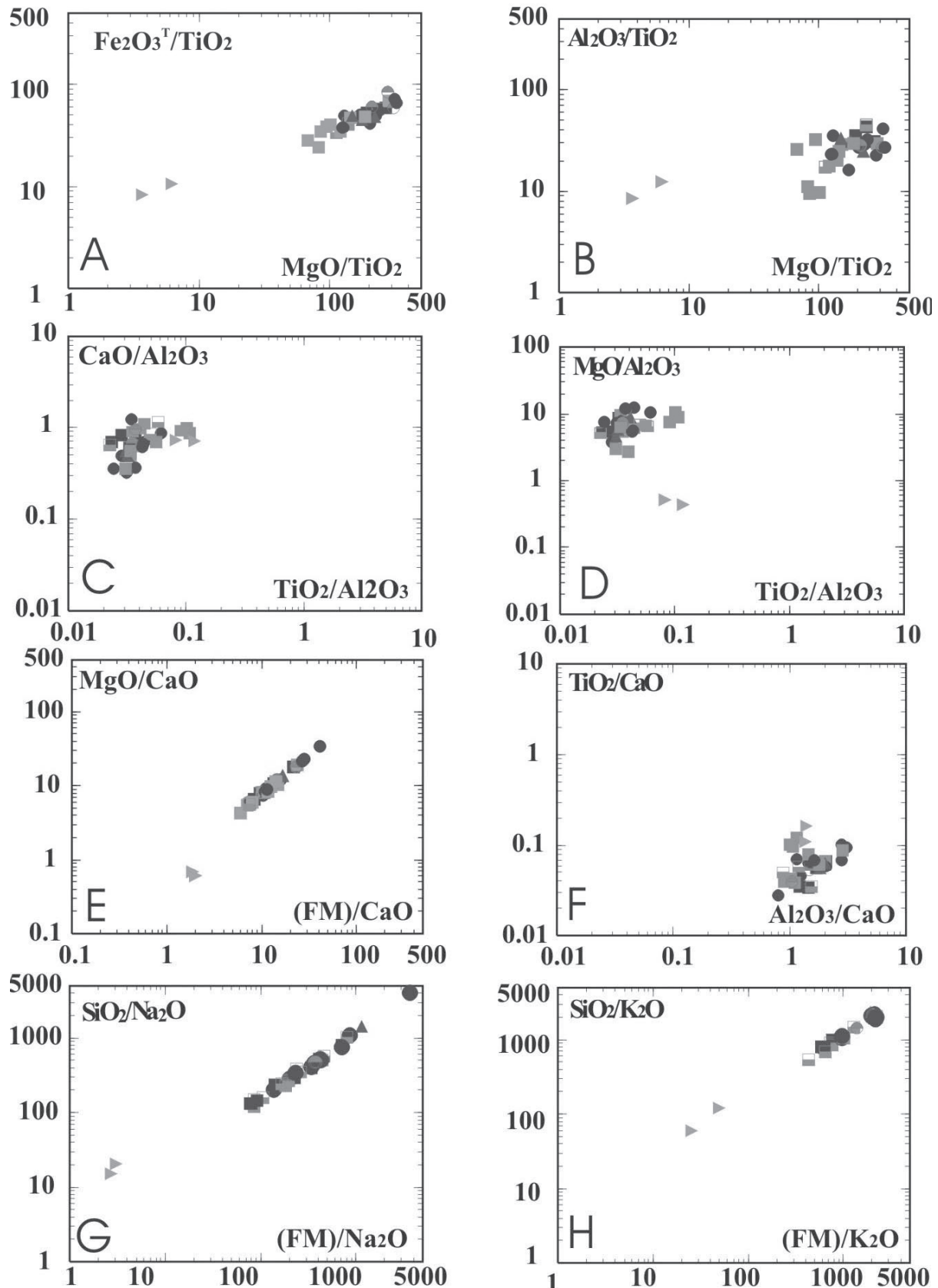


Figure 5: Diagrams representing molecular proportion ratios (RPM). Conventions: green triangle: metamafites; gray square: meta-harzburgites; blue triangle: meta-orthopyroxenite; green square: meta-websterite; gray half-square: meta-olivine-websterite; empty green circle: meta-olivine-orthopyroxenite; red half-circle: meta-lherzolite.

Table 3: Litogeochimistry of the SAI rock types (Mhz – meta-harzburgite; MlZ – meta-lherzolite; Moopx – meta-olivine-orthopyroxenite; Mwb – meta-websterite; Mowb – meta-olivine-websterite; Mpx – meta-orthopyroxenite; Mm – metabasite). Element concentrations in ppm.

	Amostra	Rb	Sn	Sr	Ta	Th	U	V	W	Zr	Y	La	Ce	Pr	Nd	Sm	Eu	Gd	Tb	Dy	Ho	Er	Tm	Yb	Lu
Mhz																									
AG03	8.30	1.00	17.60	0.10	0.70	0.10	186.00	33.10	25.20	30.30	7.70	14.30	2.04	9.20	2.70	0.59	3.10	0.79	5.22	1.15	3.51	0.64	4.36	0.65	
AG07	2.50	2.00	26.80	0.10	0.30	0.20	135.00	22.00	10.10	9.30	3.20	4.00	0.62	2.70	0.80	0.26	0.86	0.17	1.38	0.30	0.73	0.12	0.82	0.11	
AG08	5.40	2.00	62.80	0.10	0.20	0.10	106.00	20.80	6.00	18.70	4.90	2.20	0.97	5.40	1.20	0.51	1.60	0.27	1.70	0.39	1.10	0.17	0.86	0.14	
AG11	2.30	1.00	18.00	0.20	0.70	0.20	89.00	13.60	32.10	34.70	20.80	7.50	4.06	17.10	3.70	1.13	3.82	0.71	4.23	0.86	2.35	0.29	1.63	0.24	
AG13	3.60	2.00	12.30	0.10	0.20	0.10	92.00	29.10	7.00	15.90	20.40	1.60	2.41	9.30	1.40	0.27	1.85	0.34	1.88	0.43	1.22	0.15	0.76	0.13	
AG15	0.50	2.00	21.70	0.10	0.40	0.20	95.00	22.20	31.50	9.60	3.00	5.90	0.83	3.70	1.00	0.52	1.19	0.26	1.47	0.32	0.85	0.12	0.80	0.11	
AG16	1.00	1.00	22.50	0.10	0.70	0.10	75.00	29.10	25.50	6.10	2.50	5.80	0.78	4.20	0.80	0.38	1.05	0.19	1.03	0.19	0.64	0.09	0.60	0.08	
AG22	1.90	29.00	20.70	0.10	0.20	0.10	159.00	25.70	9.80	9.10	2.80	1.70	0.40	2.10	0.40	0.19	0.68	0.14	0.92	0.18	0.53	0.09	0.45	0.08	
AG59	3.90	1.00	32.50	0.10	0.10	0.10	181.00	9.80	15.40	6.70	0.60	0.90	0.16	0.80	0.30	0.12	0.58	0.13	0.83	0.24	0.66	0.11	0.61	0.11	
AG61	2.10	1.00	28.50	0.10	0.30	0.10	91.00	11.90	14.90	6.10	1.40	3.10	0.42	1.90	0.50	0.14	0.72	0.14	0.85	0.21	0.64	0.09	0.60	0.10	
AG62	3.30	2.00	23.80	0.10	0.10	0.10	92.00	9.70	16.20	5.70	1.10	2.80	0.42	2.00	0.60	0.21	0.84	0.15	0.94	0.22	0.58	0.09	0.53	0.09	
Média	3.16	4.00	26.11	0.11	0.35	0.13	118.27	20.64	17.61	13.84	6.22	4.53	1.19	5.31	1.22	0.39	1.48	0.30	1.86	0.41	1.16	0.18	1.09	0.17	
Moopx																									
AG23	3.00	2.00	52.00	0.10	0.30	0.10	96.00	37.20	10.20	4.40	0.90	1.70	0.22	1.40	0.30	0.10	0.39	0.10	0.73	0.16	0.44	0.06	0.45	0.08	
AG25	1.00	2.00	28.10	0.10	0.10	0.10	84.00	26.90	6.80	6.50	2.60	1.00	0.19	0.80	0.30	0.20	0.44	0.10	0.64	0.14	0.39	0.06	0.50	0.06	
Média	2.00	2.00	40.05	0.10	0.20	0.10	90.00	32.05	8.50	5.45	1.75	1.35	0.21	1.10	0.30	0.15	0.42	0.10	0.69	0.15	0.42	0.06	0.48	0.07	
MlZ																									
AG01	1.30	1.00	4.20	0.10	0.30	0.10	89.00	34.80	14.90	7.70	2.50	3.70	0.60	3.00	0.80	0.24	1.05	0.15	1.12	0.24	0.77	0.12	0.75	0.10	
AG12	0.80	1.00	41.40	0.10	0.10	0.10	79.00	11.90	5.60	3.30	0.80	1.10	0.15	0.90	0.40	0.21	0.32	0.07	0.47	0.11	0.31	0.05	0.29	0.04	
AG14	2.50	3.00	19.30	0.10	0.20	0.10	82.00	25.70	10.90	32.40	1.80	3.70	15.40	2.30	0.69	2.97	0.49	2.85	0.62	1.73	0.20	0.90	0.17		
AG17	3.30	2.00	17.80	0.10	0.10	0.10	131.00	35.90	11.20	6.90	1.50	0.80	0.17	0.70	0.30	0.14	0.66	0.12	0.85	0.21	0.56	0.09	0.65	0.08	
AG19	1.60	5.00	25.40	0.10	0.10	0.10	77.00	14.90	5.10	6.50	1.40	2.80	0.38	2.00	0.60	0.23	0.84	0.18	0.99	0.20	0.60	0.11	0.50	0.07	
AG21	4.50	15.00	4.30	0.10	0.20	0.10	78.00	31.00	10.10	8.70	2.50	2.80	0.49	2.20	0.50	0.16	0.73	0.12	0.95	0.22	0.60	0.09	0.57	0.09	
AG26	1.00	1.00	18.60	0.10	0.20	0.10	64.00	10.10	11.20	3.40	0.80	1.80	0.27	1.00	0.30	0.09	0.38	0.07	0.57	0.11	0.37	0.06	0.37	0.06	
AG27	4.50	1.00	28.80	0.10	0.20	0.10	110.00	25.90	14.30	126.60	32.60	2.90	3.75	15.50	2.90	0.90	5.85	0.83	4.75	1.32	3.43	0.37	1.29	0.21	
AG36	0.60	1.00	7.90	0.10	0.10	0.10	65.00	6.10	8.10	3.40	0.80	0.90	0.16	0.80	0.30	0.06	0.41	0.09	0.57	0.11	0.37	0.05	0.30	0.06	
AG63	2.90	1.00	29.00	0.10	0.30	0.10	99.00	7.60	17.50	5.80	1.60	3.70	0.48	1.90	0.60	0.15	0.83	0.15	1.04	0.20	0.60	0.08	0.60	0.09	
Média	2.30	3.10	19.67	0.10	0.18	0.10	87.40	20.39	10.89	20.47	6.79	2.23	1.02	4.34	0.90	0.29	1.40	0.23	1.42	0.33	0.93	0.12	0.62	0.10	

Table 3: Continuation.

Amostra	Rb	S _n	Sr	Ta	Th	U	V	W	Zr	Y	La	Ce	Pr	Nd	S _m	Eu	Gd	Tb	Dy	Ho	Er	Tm	Yb	Lu
Mwb																								
AG02	2.80	1.00	9.00	0.10	0.10	0.30	92.00	25.10	5.30	4.70	0.50	0.60	0.08	0.40	0.20	0.07	0.40	0.06	0.54	0.14	0.49	0.08	0.52	0.08
AG04	0.50	1.00	31.60	0.10	0.30	0.10	82.00	22.30	11.40	26.90	12.10	2.40	1.45	7.30	1.10	0.40	1.91	0.29	1.73	0.41	1.11	0.15	0.69	0.09
AG05	1.40	1.00	33.70	0.10	0.20	0.10	93.00	56.20	14.60	5.30	1.50	2.50	0.37	2.20	0.50	0.15	0.69	0.12	0.77	0.18	0.51	0.09	0.56	0.09
AG10	1.00	2.00	51.60	0.10	0.40	0.10	90.00	9.00	14.10	7.10	2.90	3.20	0.50	2.00	0.60	0.19	0.74	0.14	1.04	0.23	0.61	0.10	0.61	0.10
Média	1.43	1.25	31.48	0.10	0.25	0.15	89.25	28.15	11.35	11.00	4.25	2.18	0.60	2.98	0.60	0.20	0.94	0.15	1.02	0.24	0.68	0.11	0.60	0.09
Mowb																								
AG09	2.90	2.00	10.20	0.10	0.10	0.30	95.00	9.60	6.40	5.00	0.60	0.80	0.09	0.70	0.20	0.08	0.38	0.07	0.60	0.17	0.44	0.07	0.54	0.07
AG24	0.80	3.00	35.20	0.10	0.10	0.10	95.00	16.00	13.10	68.70	22.60	3.00	2.61	12.30	2.10	0.64	4.24	0.49	3.04	0.77	1.94	0.22	1.01	0.14
AG58	3.30	1.00	61.50	0.10	0.60	0.10	97.00	32.40	24.60	9.90	3.40	6.70	0.98	3.90	1.00	0.41	1.35	0.22	1.41	0.30	0.85	0.12	0.81	0.11
Média	2.33	2.00	35.63	0.10	0.27	0.17	95.67	19.33	14.70	27.87	8.87	3.50	1.23	5.63	1.10	0.38	1.99	0.26	1.68	0.41	1.08	0.14	0.79	0.11
Mopx																								
AG18	3.70	2.00	9.30	0.10	0.50	0.10	96.00	19.70	12.40	10.20	3.20	3.50	0.57	2.60	0.70	0.17	0.81	0.17	1.00	0.22	0.73	0.12	0.70	0.10
AG20	1.30	1.00	8.10	0.10	0.10	0.10	58.00	18.40	6.90	4.70	0.70	1.00	0.17	0.90	0.30	0.17	0.53	0.10	0.66	0.16	0.46	0.05	0.40	0.07
AG32	1.30	1.00	33.20	0.10	0.10	0.10	140.00	26.90	13.50	6.00	0.70	1.30	0.22	1.20	0.40	0.11	0.54	0.14	1.05	0.25	0.63	0.09	0.65	0.11
Média	2.10	1.33	16.87	0.10	0.23	0.10	98.00	21.67	10.93	6.97	1.53	1.93	0.32	1.57	0.47	0.15	0.63	0.14	0.90	0.21	0.61	0.09	0.58	0.09
Mm																								
AG28	16.80	1.00	174.90	0.30	0.30	0.10	267.00	76.70	57.10	31.70	6.20	10.20	1.80	8.40	2.70	1.04	3.48	0.68	4.70	1.01	2.87	0.44	2.85	0.45
AG29	16.30	1.00	144.70	0.60	0.90	0.50	342.00	172.60	100.50	51.50	11.40	21.90	3.45	16.20	4.70	1.74	6.09	1.16	6.70	1.52	4.51	0.67	3.82	0.59
Média	16.55	1.00	159.80	0.45	0.60	0.30	304.50	124.65	78.80	41.60	8.80	16.05	2.63	12.30	3.70	1.39	4.79	0.92	5.70	1.27	3.69	0.56	3.34	0.52

The multi-element diagram of Figure 8B shows that the average of REE contents for the ultramafic terms points to a differentiation level 7 times greater than the chondritic values; for the mafic terms, this factor is up to 30 times. The average values for the meta-olivine-websterite are only twice the normalizing values, which indicate that in the source region, REE concentrations would be equivalent or lower than those for the chondrite. Examining the REE concentrations for the whole of the samples, once again a question frequently posed for other Brazilian

rocks of komatiitic filiation is made. This question regards the anomalous values, sometimes higher than the chondritic (Figure 8B). This is observed in other Brazilian occurrences, such as the Mangabal I and II Complex (Candia 1982), the Morro do Ferro Volcanosedimentary Sequence (Szabó 1996), the Crixás greenstone belt komatiites (Arndt *et al.* 1989), the Rio das Velhas Supergroup magnesian and komatiitic basalts (Zucchetti 1998), the Morro da Onça komatiites (Pinheiro 1998), and the Ribeirão dos Motas Layered Sequence (Carvalho Jr. 2001).

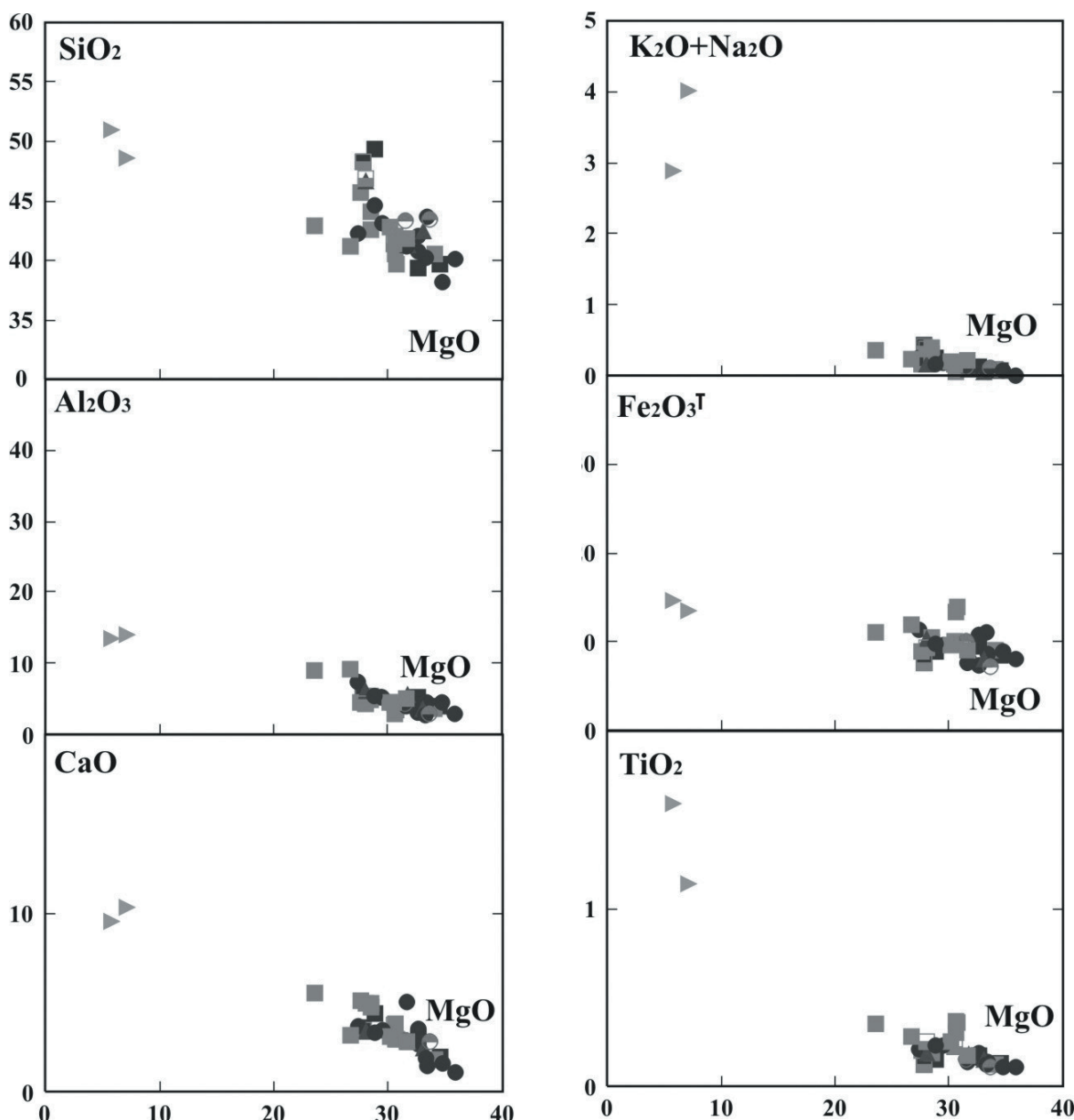


Figure 6: Bivariate diagrams, conventions as Figure 5.

When the results of the lithogeochemical analyses for each sample are correlated with the corresponding igneous layering at the outcrop scale, a repetition of the geochemical patterns results for the various rock types. This is observed in Table 4, by comparison of $[La/Yb]_n$ and $[La/Sm]_n$ ratios.

The $[La/Yb]_n$ and $[La/Sm]_n$ ratios vary respectively in the 0.69-19.25 and 1.61-9.41 intervals. In all cases, if a $[La/Yb]_n$ value is compared to the $[La/Sm]_n$ value for the same sample, one ratio never exceeds ca. 2.5 times the other ratio, implying relatively horizontal REE patterns. As there are no equivalent varieties, in terms of REE concentrations, to SAI among the classic komatiite occurrences, it is questionable that the parallelism of the average curves represented in Figure 8 should in fact represent the geochemical patterns of a primordial komatiitic magma and of the following products of fractionation of this magma. On the other hand, it would be difficult to conceive another mechanism of REE incorporation that would result in constant and proportional assimilation; contamination would lead to chaotic REE patterns. samples. Should these characteristics be inherent to the mantle source, SAI rocks would constitute a new class of komatiites. In fact, $[Gd]_n/[Yb]_n$ values can be divided in two groups: $[Gd]_n/[Yb]_n < 1$ and $[Gd]_n/[Yb]_n > 1$. The samples of the first group match with GIII-type komatiites (Al-enriched komatiites, Jahn *et al.* 1982, Figure 8C); the samples of the second group, with GI-type komatiites (Al-depleted komatiites, Jahn *et al.* 1982). Maybe this reflects both secondary Al_2O_3 mobilization processes and greater LREE assimilation by SAI rocks, fact in part corroborated by the fitting of the metamafic varieties in group GI. Similar to the population that plots in the (undefined) empty field, it could undoubtedly represent contamination with REE during the ascension and emplacement of the magmatic chambers. Another possibility would be the contamination of the magmatic source with subducted material rich in Th, Sr, Ba, Zr, Y and HREE, as suggested by Pushtel *et al.* (1993) and Condie (1994), among others.

Table 4: Ratios between oxides and REE for the SAI rock types (Mhz – meta-harzburgite; Mlz – meta-lherzolite; Moopx – meta-olivine-orthopyroxenite; Mwb – meta-websterite; Mowb – meta-olivine-websterite; Mpx – meta-orthopyroxenite; Mm – metamafile). See reference on $[La]_n/[Yb]_n$, $[La]_n/[Sm]_n$ and $[Gd]_n/[Yb]_n$ normalization in the text.

Amostra	CaO Al_2O_3	Al_2O_3 TiO_2	$[La]_n$ $[Yb]_n$	$[La]_n$ $[Sm]_n$	$[Gd]_n$ $[Yb]_n$
Mhz					
AG03	0.62	25.66	1.27	1.84	0.59
AG07	0.90	28.74	2.80	2.58	0.87
AG08	1.11	22.90	4.09	2.64	1.54
AG11	0.86	9.42	9.15	3.63	1.94
AG13	0.50	29.50	19.25	9.41	2.01
AG15	0.93	11.00	2.69	1.94	1.23
AG16	0.99	9.80	2.99	2.02	1.45
AG22	0.97	24.50	4.46	4.52	1.25
AG59	0.35	32.46	0.71	1.29	0.79
AG61	0.56	29.65	1.67	1.81	0.99
AG62	0.70	17.84	1.49	1.18	1.31
Média	0.72	20.52	4.08	3.30	1.12
Moopx					
AG23	0.67	28.47	1.43	1.94	0.72
AG25	0.95	26.91	3.73	5.59	0.73
Média	0.78	27.85	2.64	3.77	0.72
Mlz					
AG01	0.81	27.25	2.39	2.02	1.16
AG12	0.86	16.32	1.98	1.29	0.91
AG14	0.32	32.43	18.65	6.57	2.73
AG17	0.49	35.52	1.66	3.23	0.84
AG19	1.24	29.00	2.01	1.51	1.39
AG21	0.69	22.50	3.15	3.23	1.06
AG26	0.35	41.09	1.55	1.72	0.85
AG27	0.66	23.00	18.13	7.26	3.75
AG36	0.36	26.82	1.91	1.72	1.13
AG63	0.61	23.39	1.91	1.72	1.14
Média	0.62	27.75	7.83	4.87	1.87
Mwb					
AG02	0.69	43.25	0.69	1.61	0.64
AG04	0.49	30.62	12.58	7.10	2.29
AG05	0.82	35.33	1.92	1.94	1.02
AG10	0.59	30.29	3.41	3.12	1.00
Média	0.66	35.07	5.12	4.57	1.30
Mowb					
AG09	0.65	44.67	0.80	1.94	0.58
AG24	0.84	20.27	16.05	6.95	3.47
AG58	1.15	17.28	3.01	2.19	1.38
Média	0.86	23.55	8.08	5.20	2.09
Mpx					
AG18	0.50	31.22	3.28	2.95	0.96
AG20	0.65	24.67	1.26	1.51	1.10
AG32	0.55	32.68	0.77	1.13	0.69
Média	0.56	30.47	1.89	2.12	0.89
Mm					
AG28	0.73	12.34	1.56	1.48	1.01
AG29	0.71	8.42	2.14	1.57	1.32
Média	0.72	10.02	1.89	1.54	1.19

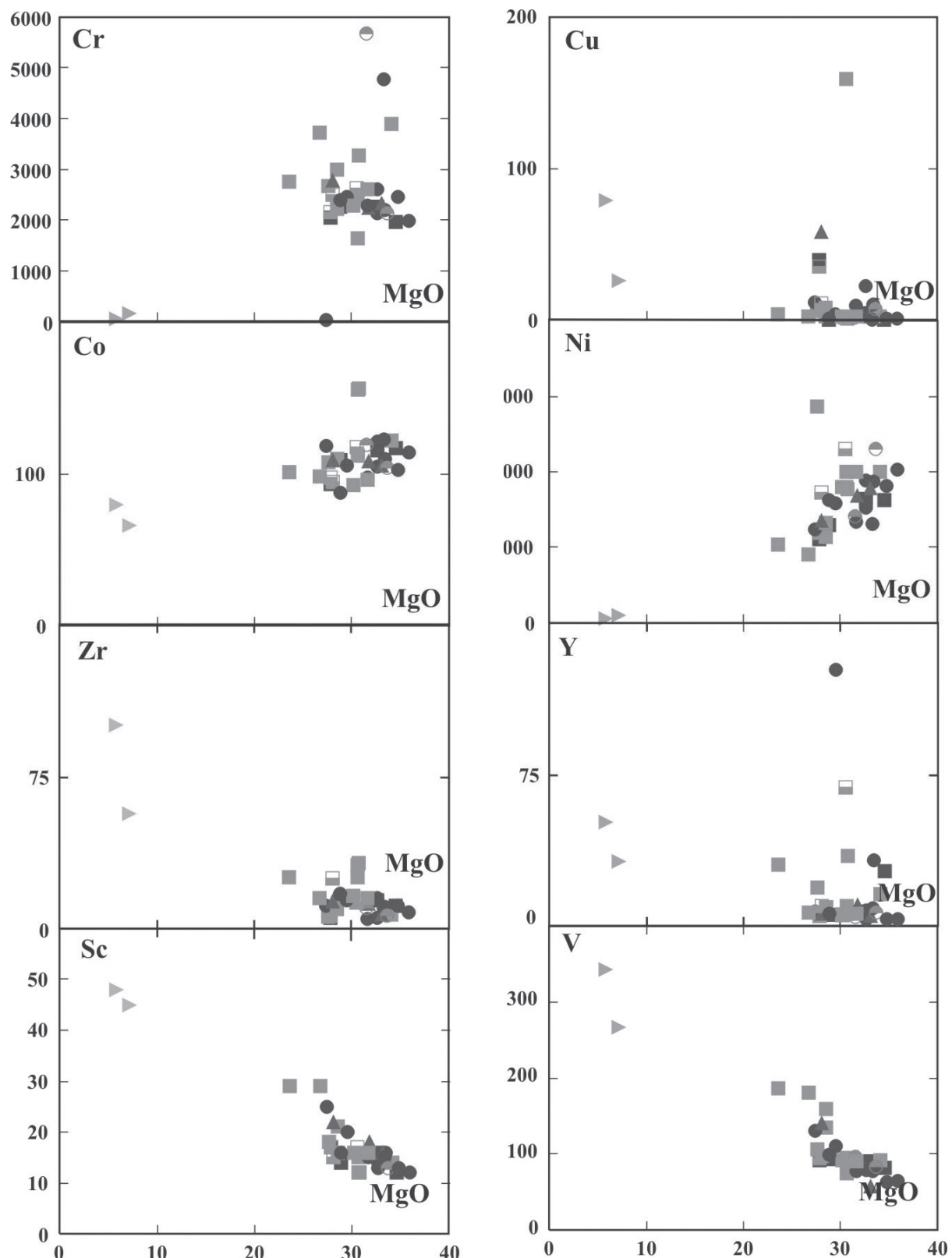


Figure 7: Bivariate diagrams, conventions as Figure 5.

DISCUSSION

The SAI most preserved ultramafic rock types are predominantly ultrabasic ($\text{SiO}_2 < 45\%$ – see Table 1). Some samples, however

(e.g. AG02, 05, 08, 09, 32 and 58 – see Table 1), exhibit increased SiO_2 concentrations, so that primordial ultramafic rocks of ultrabasic character now present SiO_2 contents typical of basic rocks. This is due to metamorphic/

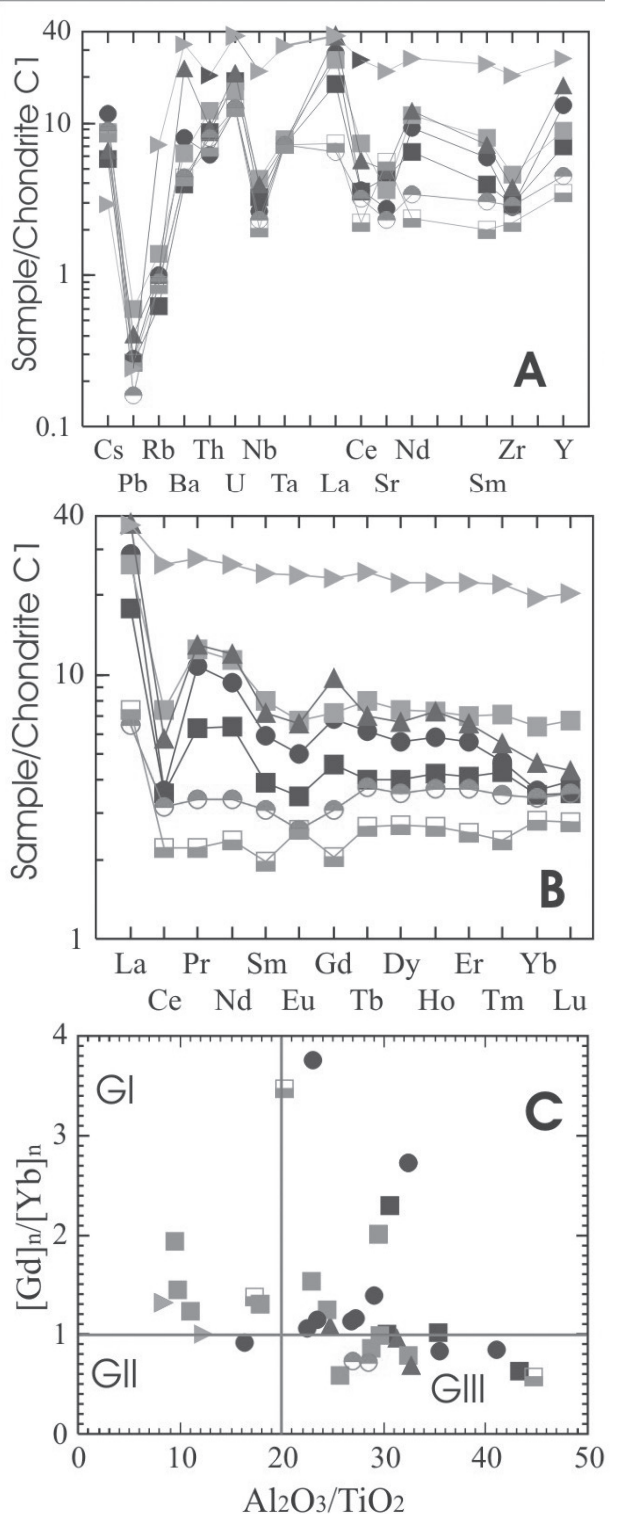


Figure 8: A) Multi-element diagram showing the SAI geochemical pattern. B) Multi-element diagram showing the SAI REE pattern; C) Arndt (1994) diagram for classification of komatiitic suites, adapted from Jahn et al. (1982). Diagrams A and B normalized to C1 chondrite (Sun & McDonough 1989); $[Gd]_n$ and $[Yb]_n$ normalized to primitive mantle values (Sun & McDonough 1989). GI – Barberton-type komatiites; GII – Munro-type komatiites; GIII – Gorgona-type komatiites. Conventions as Figure 5.

metasomatic processes that affected the SAI rock types. As a consequence, the normative composition of some samples is not coherent with their modal composition. This may have resulted from the chemical mobility of some elements (e.g. Si or Mg). According to the norm, the samples are classified as lherzolites, harzburgites, olivine-orthopyroxenites, olivine-websterites, olivine-gabbro and gabbronorite (Figures 9A and 9B).

Additionally modal compositions also yielded websteritic and orthopyroxenitic compositions. Regarding the nature of the primordial magmas that generated SAI, the Morro da Onça komatiitic metavolcanites, which may be a possible continuity of SAI northeastwardly, indicate that both the Morro da Onça metakomatiites and the SAI metaultramafites would have originated from the same parental magma of komatiitic nature. Should this be the case, these occurrences would represent distinct crustal environments of the same unit. SAI would represent the plutonic and the Morro da Onça flows the volcanic terms of this magmatism. In time, this ultramafic magmatism could have taken place continuously throughout the Rio das Velhas Tectonothermal Event or at various steps, as attested by the contact aureoles preserved in metasedimentary rocks south of SAI. According to the $MgO-CaO-Al_2O_3$ and $MgO-NaO-K_2O-FeO$ systems (Figures 9C and D), the samples evidence characteristics both of ophiolitic cumulates and rocks of komatiitic filiation. This is also observed in the Quebra Ossos Group komatiites of the Rio das Velhas Supergroup (Schorscher, 1992). Despite the fact that the alpine peridotites and rocks of komatiitic filiation present similar compositions in certain aspects, Figure 9E also indicates a possible komatiitic filiation for the SAI parental magmas. In this diagram, the samples plot in the field of the komatiitic suites and define a characteristic trend distributed between peridotitic komatiite and komatiitic basalt sub-fields. In the latter sub-field, the samples plot close to the limit of the high-Fe tholeiite field. When classification parameters for komatiitic varieties are

analyzed, as the CaO/Al₂O₃ and Al₂O₃/TiO₂ ratios, the samples of ultramafic composition yield CaO/Al₂O₃ values between 0.32 and 1.24 and Al₂O₃/TiO₂ values between 16.31 and 44.66. In these aspects, SAI is similar to the Bushveld komatiitic ultramafites (Cawtorn & Davies, 1982), the Barbeton cumulitic ultramafites (Brooks & Hart 1974, Nesbit *et al.* 1979, Jahn *et al.* 1982) and the Phanerozoic Gorgona Island komatiites (Echeverria, 1982). The gabbroic terms, despite being a differentiated phase in the context of the layered sequence, yield CaO/Al₂O₃ ratios close to the values for komatiitic basalts. Therefore, the SAI mafic rocks are similar to kindred rocks from Barbeton (Brooks & Hart, 1974), Gorgona Island (Echeverria, 1982) or even to Phanerozoic tholeiites (Cameron & Nisbet, 1982). To Arndt (1994), the use of the CaO/Al₂O₃ ratio to characterize komatiites is questionable, once CaO is mobile, whereas Al₂O₃ is an important parameter in the study of komatiitic magma compositions. The Al₂O₃/TiO₂ ratio is much more representative, due to the relative TiO₂ immobility in the majority of the metamorphic/metasomatic processes. According to Al₂O₃/TiO₂, the SAI samples are divided in two distinct populations: the first having Group I characteristics (Al-depleted komatiites with [Gd]_n/[Yb]_n > 1 or Barbeton-type; Jahn *et al.* 1982), and the second having Group III characteristics (Al-enriched komatiites with [Gd]_n/[Yb]_n < 1 or Gorgona-type, Jahn *et al.*, 1982). Taking the metamafites and assuming a possible "basaltic-komatiitic" chemical affinity, these rocks plot in Figure 8C together with the Group I population (Barbeton-type komatiites). This information suggests a possible komatiitic affinity for the SAI parental magmas.

CONCLUSION

According to the previous items, SAI presents preserved igneous characteristics, both macroscopic and microscopic, which classifies it as a layered sequence. Macroscopically, the compositional layering stands out, with the cyclic alternation of

rock types that vary from peridotitic to gabbroic terms. Under the microscope these characteristics are expressed in the partially intact cumulitic textures, despite of the high-grade metamorphism that affected them. There are also the subtle records of contact aureoles, preserved in the fragments of the meta-volcanosedimentary unit. Geochemically, despite the mobility of some elements, the fractionation relations between oxides and elements as a function of MgO variations seem to preserve a large part of their geochemical evolution history. This evolution is observed in the fractionation patterns obtained from bivariant diagrams and constitute fractionation patterns perfectly expected for magnesian magmas, such as komatiitic magmas. Cr, Ni and Co variations with decreasing MgO stand out among these fractionation patterns. As previously mentioned, Cr behaves as a compatible element for MgO contents less than 25% in the residual liquid, which explains the relations between the fractionation of olivine and chromite as conspicuous phases during magma differentiation. It should be stressed out that a campaign to study the SAI cyclic units in detail is still necessary for the elaboration of more consistent metallogenetic models. However, the data presented here already point to geochemical conditions necessary for the precipitation of at least disseminated chromite levels. Similarly, the behavior of Ni and Co as compatible elements suggests a possible metallogenetic potentiality associated with the precipitation of massive or disseminated sulfide levels. The SAI fractionation patterns correspond to those for primitive magnesian magmas, such as the komatiitic magmas. This fact, in addition to the data here presented, suggests that the parental magma that originated SAI is of komatiitic filiation. The [Gd]_n/[Yb]_n and Al₂O₃/TiO₂ ratios play an important role in this discussion and are adopted as classification parameters to discriminate the known komatiitic varieties. In this sense, SAI presents characteristics oscillating between Al-depleted or Al-enriched komatiites. SAI rocks also show rather

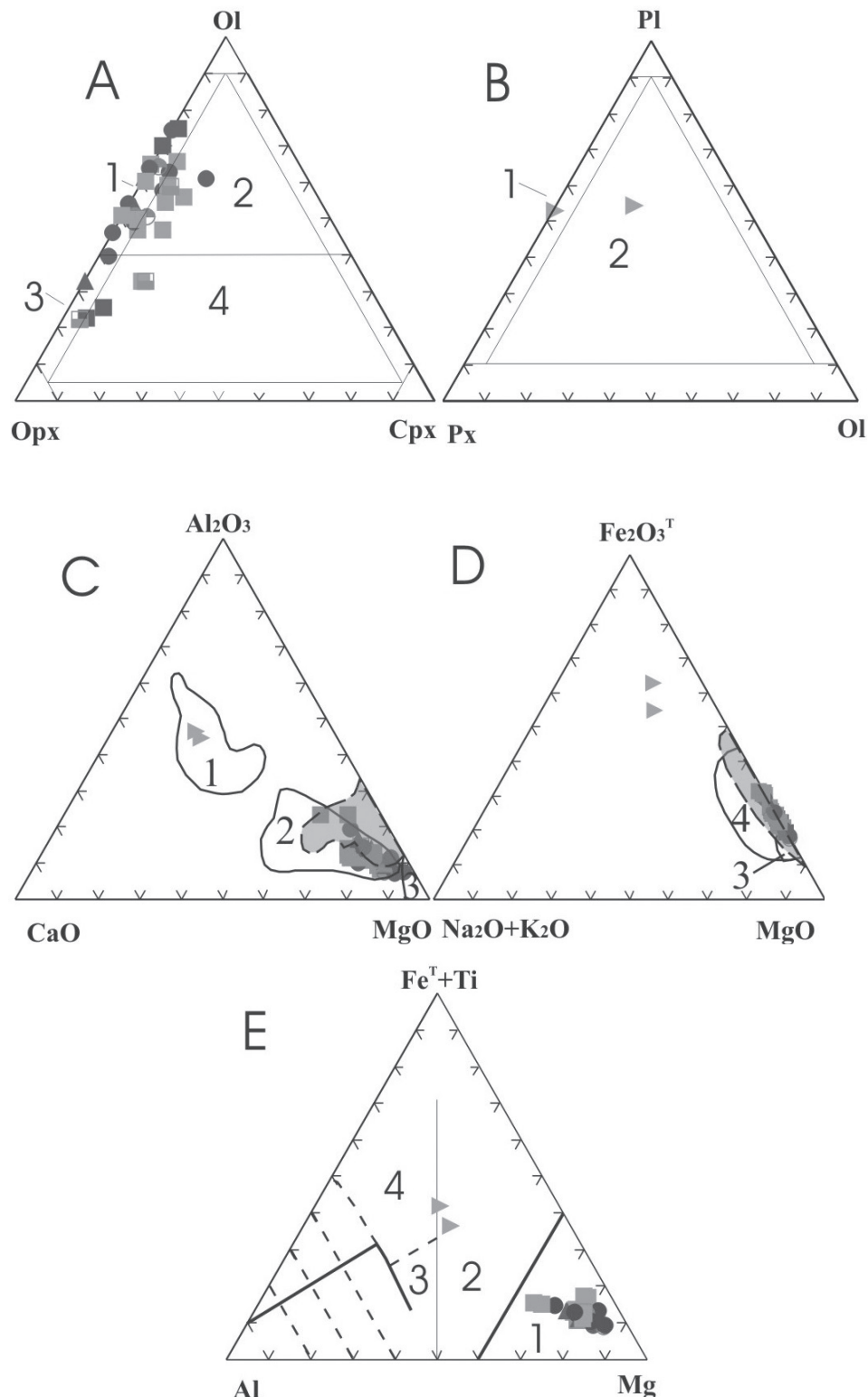


Figure 9: A) Streckeisen (1976) diagram for ultramafic rocks. 1 - harzburgites; 2 - lherzolite; 3 - olivine-orthopyroxenite; 4 - olivine-websterite. B) Streckeisen (1976) diagram for mafic rocks. 1 - gabbro, gabbronorite, norite; 2 - olivine gabbro, olivine gabbronorite, olivine norite. C) and D) Coleman (1977) discriminant diagrams for ultramafic rocks, according to Fe_2O_3^T , $\text{Na}_2\text{O}+\text{K}_2\text{O}$, MgO , CaO and Al_2O_3 percentages. Fields: 1 – ophiolite mafic cumulates; 2 - ophiolite ultramafic cumulates; 3 - ophiolite metamorphic peridotites; 4 – ophiolite cumulitic mafic and ultramafic rocks. Hatched area in yellow: Quebra Ossos Group komatiites (Schorscher 1992). E) Jensen (1976) discriminant diagram, corrected by Rickwood 1989), for komatiitic, tholeiitic and calc-alkaline suites. Fields: 1 – peridotitic komatiites; 2 – komatiitic basalts; 3 – high-Mg tholeiites; 4 – high-Fe tholeiites. Conventions as Figure 5.

particular REE anomalies, indicating two possible interpretations: 1) these anomalies would result from secondary processes as assimilation of crustal components; 2) these anomalies would constitute a characteristic inherent and particular of , de the mantle source in question. This last hypothesis seems to be more adequate because the geochemical patterns between distinct samples are very regular and therefore the high REE concentrations could be a primordial characteristic of the parental magmas. The anomalies observed in SAI were also detected in other kindred Brazilian occurrences (Candia 1982, Szabó 1996, Arndt *et al.* 1989, Zucchetti 1998, Pinheiro 1998, Carvalho Jr. 2001). These characteristics put in evidence the possibility of a mantle source naturally more REE-enriched or metasomatically modified by geochemical crustal components, during recycling episodes. Another factor may be associated with this last hypothesis, which is the possibility of mantle hydration for the generation of komatiitic magmas. To support this line of investigation, the

hornblendites, taken as a SAI petrographic variety, should be studied in detail. Simple crustal assimilation processes are not ruled out and could also have contributed to the SAI petrogenetic evolution. Besides the geochemical evidences, this hypothesis is supported by field relations that indicate the presence of xenoliths of felsic rocks, gneisses, and even rare ultramafites, among the SAI cyclic mafic-ultramafic units. This in turn would strengthen the idea that the ultramafic magmatism of the southern São Francisco Craton occurred continuously throughout the Rio das Velhas Tectono-thermal Event and, in this case, SAI would possibly represent one of its last manifestations.

ACKNOWLEDGMENTS

The authors wish to thank Fundação de Amparo a Pesquisa do Estado de Minas Gerais (FAPEMIG), Processes CRA 619/04 and CRA 2032/05; and Conselho Nacional de Desenvolvimento Científico e Tecnológico (CNPq) for the financial support to this study.

REFERENCES

- ALKMIN F.F., MARSHAK S. (1998) Transamazonian Orogeny in the Southern São Francisco Craton Region, Minas Gerais, Brazil: evidence for Paleoproterozoic collision and collapse in the Quadrilátero Ferrífero. *Precambrian Research*, 90: 29-58.
- ARNDT N.T. (1994) Archean Komatiites. Condie K. C. (Ed). *Archean Crustal Evolution*, Elsevier. p. 11-44.
- ARNDT N.T. & NISBET R.W. (1982) What is a komatiíte? In: Arndt N. T, Nisbet E. G (Eds). *Komatiites*. George Allen & Unwin, p. 19-28.
- ARNDT N.T, TEIXEIRA N.A. & WHITE W.M. (1989) Bizarre geochemistry of komatiites from the Crixás greenstone belt, Brazil. *Contribution in Mineralogy & Petrology*, 101: 187-197.
- BINNS R.A., HALLBERG J.A., TAPLIN J.H. (1982) Komatiites in the Yilgarn Block, Western Austrália. In: Arndt N. T. & Nisbet E.G. (Eds) *Komatiites*. George Allen & Unwin, p. 117-130.
- BROOKS C. & HART S.R. (1974) On the significance of Komatiite. *Geology*, 2: 107-110.
- CAMERON W.E. & NISBET E.G. (1982) Phanerozoic analogues of komatiitic basalts. In: Arndt N.T, Nisbet E.G (Eds). *Komatiites*. George Allen & Unwin, p. 29-50.

CAMPOS J.C.C. (2004). O lineamento Jeceaba – Bom Sucesso como Limite dos Terrenos Arqueanos e Paleoproterozóicos do Cráton São Francisco Meridional: Evidências Geológicas, Geoquímicas (Rocha Total) e Geocronológicas (U–Pb). Tese de Doutoramento, Departamento de Geologia, Escola de Minas, Universidade Federal de Ouro Preto, Ouro Preto, 189 p.

CAMPOS J.C.S., CARNEIRO M.A., BASEI M.A.S. (2003) U-Pb evidence for Late Neoarchean crustal reworking in the southern São Francisco Craton (Minas Gerais, Brasil). *Anais da Academia Brasileira de Ciências*, 75: 497-511.

CANDIA M.A.F. (1983) Petrologia dos Complexos Máfico-Ultramáficos de Mangabal I e II, Sanclerlândia, Goiás. Tese de Doutoramento. Instituto de Geociências da Universidade de São Paulo, São Paulo, 400p.

CARNEIRO M.A. (1992) O Complexo Metamórfico Bonfim Setentrional (Quadrilátero Ferrífero, Minas Gerais): Litoestratigrafia e Evolução Geológica de um Segmento de Crosta Continental do Arqueano. Tese de Doutoramento, Instituto de Geociências, Universidade de São Paulo, 233 p.

CARNEIRO M.A., CARVALHO Jr. I.M., TEIXEIRA W. (1998a) Petrologia, geoquímica e geocronologia dos diques máficos do Complexo Bonfim Setentrional (Quadrilátero Ferrífero) e suas implicações na evolução crustal do Cráton São Francisco Meridional. *Revista Brasileira de Geociências*, 28: 29-44.

CARNEIRO M.A., ENDO I., NALINI Jr. H.A., SALES J.C.C., GOULART L.E.A., SILVA E.F., PEREIRA A.A., TAVARES T.D., JIAMELARO F., CARNEIRO J.M., MARIANO L.C., PRADO G.E.A., URBANO E.P.C., SANTOS C., MIGUEL F.P. (2006) Folhas Campo Belo e Oliveira (1:100.000). Convênio CPRM/UFOP.

CARNEIRO M.A., GROSSI SAD J.H., CARVALHO Jr I.M., NALINI Jr. H.A., LIMA J.F., CAMPOREZ J.A.P., TEIXEIRA W. (1999) Possible Komatiitic Affinity and Potencial PGE Mineralization of the Archean Ribeirão dos Motas Layered Sequence, Brasil. In: Third International Workshop on Orogenic Lherzolites and Mantle Processes. Pavia, Italy, Abstr., 24: 80-81.

CARNEIRO M.A., NALINI Jr. H.A., BILALE, CARVALHO Jr. I.R., TEIXEIRA W., MOUTTE J. (1997a) A Seqüência Acamada Ribeirão dos Motas, Minas Gerais, Brasil. In: X Semana de Geoquímica, IV Congresso de Geoquímica dos países de Língua Portuguesa, Braga, Atas, p. 31-33.

CARNEIRO M.A., TEIXEIRA W., CARVALHO Jr. I.M., OLIVEIRA A.H., FERNANDES R.A. (1997b) Archean Sm/Nd isochron age from the Ribeirão dos Motas layered rocks sequence, Southern São Francisco-Craton, Brazil. In: South-American Symposium on Isotope Geology, SBG, Extended Abstracts, p. 63-64.

CARNEIRO M.A., TEIXEIRA W., CARVALHO Jr. I.M., FERNANDES R.A. (1998b) Ensialic tectonic setting of the Archean Rio das Velhas Greenstone Belts: Nd and Pb isotopic evidence from the Bonfim Metamorphic complex, Quadrilátero Ferrífero, Brazil. *Revista Brasileira de Geociências*, 28: 189-200.

- CARNEIRO M.A., TEIXEIRA W., NALINI Jr. H.A., BILALE E., OLIVEIRAA.H., CARVALHO Jr. I.R. (1996) Archean ultramafic-mafic magmatism in the Southern São Francisco Craton (Campo Belo Complex): Preliminary petrographic and geochemical results. In: Symposium on Archean Terranes of the South American Plataform, SBG, Anais, p. 32-33.
- CARVALHO Jr I.M. (2001) Petrologia e Geologia de Rochas Ultramáficas Arqueanas do Cráton São Francisco Meridional: A Seqüência Acamada Ribeirão dos Motas. Dissertação de Mestrado. Departamento de Geologia, Escola de Minas, Universidade Federal de Ouro Preto, 96 p.
- CARVALHO Jr I. M. & CARNEIRO M.A (1999) Modelo petrogenético para os anfibólios ígneos intercúmulos da Seqüência Acamadada Ribeirão dos Motas. Pesquisa e Pós Graduação, UFOP, 32 p.
- CARVALHO Jr I.M., CARNEIRO M.A., FERNANDES R.A., TEIXEIRA W. (1998a) Processos mantélicos relacionados à gênese da estratificação ígnea da Seqüência Acamadada Ribeirão dos Motas. In: SBG, Congresso Brasileiro de Geologia, 40: Resumos, p. 67.
- CARVALHO Jr I.M., CARNEIRO M.A., NALINI Jr. H.A., TEIXEIRA W. (1998b) Seriam as Rochas da Seqüência Acamadada Ribeirão dos Motas o Correspondente Plutônico do Magmatismo Ultramáfico do Greenstone Belt Rio das Velhas? In: Congresso Brasileiro de Geologia, 40, Belo Horizonte. Resumos, p. 68.
- CAWTHORN R.G. & DAVIES G. (1982) Possible Komatiitic Affinity of the Bushweld Complex, South Africa. In: Arndt N.T & Nisbet E.G (Eds). Komatiites. 6, London, George Allen & Unwin. p. 91-96.
- COLEMAN R.G. (1977) Ophiolites: Ancient Oceanic Lithosphere? Springer-Verlag, Berlin, 228 p.
- CONDIE K.C. (1994) Greenstone through time. In: Condie K. C. (Ed). Archean Crustal Evolution. Amsterdan, Elsevier. p. 85-120.
- CORDANI U.G., SATO K., TEIXEIRA W., TASSINARI C.C.G., BASEI M.A.S. (2000) Crustal Evolution of South American Platform. In: CORDANI U. G., MILANI E.J., THOMAZ FILHO A. & CAMPOS D.A. (eds.). Tectonics Evolution of South America. ABC/DNPM/MCT, p. 19-40.
- COSTA C.S. (1995) Petrogênese do Corpo Metaultramáfico do Córrego dos Boiadeiros, Quadrilátero Ferrífero, Minas Gerais, Brasil. Dissertação de Mestrado. Belo Horizonte, UFMG, 172 p.
- COUTO D.J.F. (2004) Petrogênese dos Metaultramafitos e Mafitos da Região de Cláudio (MG). Dissertação de Mestrado. Departamento de Geologia, Escola de Minas, Universidade Federal de Ouro Preto, 173 p.
- COUTO D.J.F. & CARNEIRO M.A. (2007) Gênese dos Metaultramafites from Cláudio (MG). *Geochimica Brasiliensis*, 21: 9-21.
- ECHEVERRIA L.M. (1982) Komatiites from Gorgona Island, Colômbia. In: Arndt N. T, Nisbet E. G (Eds). Komatiites. George Allen & Unwin. p. 91-96.

- ENDO I., CARNEIRO M.A., MACHADO R. (1996) O Complexo Metamórfico Bação: Um elemento anisotrópico na deformação do Supergrupo Rio das Velhas – Q.F., MG. In: Congresso Brasileiro de Geologia, 39, Salvador, 1996. Anais, 1: 411-413.
- FERNANDES R.A. (2001) Etapas de Formação de Crosta Continental (do Mesoarqueano ao Mesoproterozóico) no Cráton São Francisco Meridional. Dissertação de Mestrado. Departamento de Geologia da Escola de Minas, Universidade Federal de Ouro Preto, Ouro Preto, Ouro Preto, 127 p.
- GOULART L.E.A. (2006) O Complexo Acamadado Itaguara Rio-Manso. Dissertação de Mestrado. Departamento de Geologia da Escola de Minas, Universidade Federal de Ouro Preto, Ouro Preto, Ouro Preto, 178 p.
- HOFMANN A.W. (1988) Chemical differentiation of the Earth: the relationships between mantle, continental crust and oceanic crust. *Earth and Planetary Science Letters*, 90: 297-314.
- IRVINE T.N. (1975) Crystallization sequences in the Muskox intrusions and other layered intrusions. II. Origin of the cromitite layers and similar deposits of the other magmatic ores. *Geochimica et Cosmochimica Acta*, 39: 991-1020.
- IRVINE T.N. (1977) Crystallization sequences in the Muskox intrusions and other stratiform intrusions: A new interpretation. *Geology*, 5: 273-277.
- JAHN B.M., GRUAU G., GLICKSON A.Y. (1982) Komatiites de Onverwacht Group, South Africa: REE chemistry, Sm-Nd age and mantle evolution. *Contributions in Mineralogy & Petrology*, 80: 25-40.
- JENSEN L.S. (1976) A new method of classifying subalcalic volcanic rocks. Ontario Division of Mines, Misc. Paper, 66.
- LE MAITRE R.W., BATEMAN P., DUDEK A., KELLER J., LE BAS M.J., SABINE P.A., SCHMID R., SORENSEN H., STRECKEISEN A., WOOLLEY A.R., ZANETTIN B. (1989) A classification of igneous rocks and glossary of terms. Oxford, Blackwell.
- MACHADO N. & CARNEIRO M. A. (1992) U-Pb evidence of late Archean tectono-thermal activity in the Southern São Francisco Shield, Brazil. *Canadian Journal of Earth Science*, 29: 2341-2346.
- NALDRETT A.J. & VON GRUENEWALD G. (1989) The association of PGE with chromitite in layered intrusions and ophiolite complexes. *Economic Geology*, 84: 102-144.
- NESBITT R.W., SUN S.S., PURVIS A.C. (1979) Komatiites: geochemistry and genesis. *Canadian Mineralogist*, 17: 165-186.
- NOCE C.M. (1995) Geocronologia dos eventos magmáticos, sedimentares e metamórficos na região do Quadrilátero Ferrífero, Minas Gerais. Tese de Doutoramento. Instituto de Geociências, Universidade de São Paulo, São Paulo, 128 p.
- PADILHA A.V. (1984) Formação Córrego dos Boiadeiros – Uma seqüência komatiítica na base do Grupo Nova Lima, Supergrupo Rio das Velhas, MG. In: SBG, Congresso Brasileiro de Geologia, 33, SBG, Anais p. 2668-2669.

- PINHEIRO S.O. (1998) Petrologia das rochas meta-ultramáficas da região de Rio Manso, Minas Gerais. Tese de doutoramento. Instituto de Geociências, Universidade de Brasília, Brasília, 253 p.
- PUCHTEL I.S., BOGATIKOV O.A., SIMON A.K. (1993) The Early Precambrian crust-mantle evolution of the Olekma gneiss-greenstone terrane, Aldan Shield. *Petrology*, 1: 451-473.
- RICKWOOD P.C. (1989) Boundary lines within petrologic diagrams which use oxides of major and minor elements. *Lithos*, 22: 247-263.
- ROLLINSON H. (1993) Using Geochemical Data: Evaluation, Presentation, Interpretation. 1^a Ed, Longman Scientific & Technical, 312 p.
- SCHORSCHER H.D. (1992) Arcabouço Petrográfico e Evolução Crustal de Terrenos Pré-Cambrianos do Sudoeste de Minas Gerais: Quadrilátero Ferrífero, Espinhaço Meridional e domínios Granito-Gnássicos adjascentes. Tese de Livre Docência. Instituto de Geociências, Universidade de São Paulo, São Paulo, 178p.
- SCHORSCHER H.D, CHIARINI A.P., FERNANDES F., VILELA L.G.G., MONTEIRO L.V.S., SILVA E.L., CUTRIM C.A. (1998) Revisão tectono estratigráfica do Maciço de Piumhi-MG. In: Congresso Brasileiro de Geologia, 40, Belo Horizonte, SBG, Resumos, 68.
- SCHRANK A., SOUZA FILHO C.R., ROIG H.L. (1990) Novas observações sobre as rochas ultramáficas do Grupo Quebra Osso e Formação Córrego dos Boiadeiros, “Greenstone Belt” Rio das Velhas (MG). *Cadernos IG/UNICAMP*, 1:6-29.
- SMITH H.S., ERLANK A.J., DUNCAN A.R. (1980) Geochemistry of some ultramafic komatiite lava flows from the Barberton Mountain Land. *South Africa Precambrian Research*, 11: 399-415.
- STRECKEISEN A. (1976) To each plutonic rock its proper name. *Earth Sciences Review*, 12: 1-33.
- SUN S.S. & McDONOUGH W.F. (1989). Chemical and isotopic systematics of oceanic basalts: implications for mantle composition and processes. In: Sunders A.D. & Norry M.J. (Eds). *Magmatism in Ocean Basins*. Geological Society of London Special Publications, 4242: 313-345.
- SZABÓ G.A.J. (1996) Petrologia das Suíte Metalultramáfica da Seqüência Vulcano-sedimentar Morro do Ferro na região de sul a oeste de alpinópolis, Minas Gerais (Domínio Norte do Complexo Campos Gerais). Tese de Doutoramento. Instituto de Geociências, Universidade de São Paulo, São Paulo, 354 p.
- TEIXEIRA W. (1985) A Evolução Geotectônica da Porção Meridional do Cráton São Francisco, com Base em Interpretações Geocronológicas. Tese de Doutoramento. Instituto de Geociências, Universidade de São Paulo, São Paulo, 207 p.
- TEIXEIRA W., CARNEIRO M.A., NOCE C.M., MACHADO N., SATO K., TAYLOR P.N. (1996) Pb, Sr and Nd Isotope Constraints on the Archean Evolution of Gneissic-granitoid

Complexes in the Southern São Francisco Craton, Brazil. Precambrian Research, 78:151-164.

TEIXEIRA W., SABATÉ P., BARBOSA J., NOCE C.M., CARNEIRO M.A. (2000) Archean and Paleoproterozoic Tectonic Evolution of the São Francisco Craton. In: Cordani, U. G. Milani, E. J. Thomaz Filho & Campos, D. A. Tectonic Evolution of South America. p. 101-137.

VALENÇA J.G., PACIULO F.V.P., RIBEIRO A.E., ANDREIS R.R. (1998) Komatiítos da Fazenda Chapadinha, Faixa Greenstone Itumirim-Tiradentes, Borda Sul do Craton São Francisco, Minas Gerais. In: Congresso Brasileiro de Geologia, 40, SBG, Belo Horizonte, Resumos, p. 62.

VILJOEN M.J. & VILJOEN R.P. (1969) The geology and geochemistry of the lower ultramafic unit of the Onverwacht Group and a proposed new class of igneous rock. Special Publication of the Geological Society of South Africa, 2: 221-244.

WAGER L.R. & BROWN G.M. (1976) Layered Igneous Rocks. Oliver & Boyd. 588 p.

WILSON M. (1989). Igneous Petrogenesis. Harper Collins Academic, 466 p.

ZUCCHETTI M. (1998) Geoquímica dos Metabasaltos do Grupo Nova Lima, Greenstone Belts Rio das Velhas, Quadrilátero Ferrífero, Minas Gerais. Dissertação de Mestrado. Instituto de Geociências, Departamento de Geologia, Universidade de Minas Gerais, 207 p.

(Footnotes)

¹To whom the correspondence should be sent: mauricio@degeo.ufop.br